A systematic framework for using membrane metrics for strain engineering

Miguel C. Santoscoy[1] and Laura R. Jarboe[1*]

[1]Department of Chemical and Biological Engineering, Iowa State University, Ames, IA 50011. USA

* To whom correspondence should be addressed: ljarboe@iastate.edu. 515-294-2319

HIGHLIGHTS

- Differential gene expression of *fabA*, *fabB* or *des* impacted various membrane metrics.

- Effect of some microbial inhibitors on membrane metrics and growth was quantified.

- Membrane metrics to predict growth are recommended for seven combined conditions.

- Growth at 42 °C with furfural and ethanol corresponds to membrane hydrophobicity.

- Membrane hydrophobicity correlated to ethanol production in the combined condition.

ABSTRACT

The cell membrane plays a central role in the fitness and performance of microbial cell factories and therefore it is an attractive engineering target. The goal of this work is to develop a systematic framework for identifying membrane features for use as engineering targets. The metrics that describe the composition of the membrane can be visualized as "knobs" that modulate various "outcomes", such as physical properties of the membrane and metabolic activity in the form of growth and productivity, with these relationships varying depending on the condition. We generated a set of strains with altered membrane lipid composition via expression of *des*, *fabA* and *fabB* and performed a rigorous characterization of these knobs and outcomes across several individual inhibitory conditions. Here, the knobs are the relative abundance of unsaturated lipids and lipids containing cyclic rings; the average lipid length, and the ratio of linear and non-linear lipids (L/nL ratio). The outcomes are membrane permeability, hydrophobicity, fluidity, and specific growth rate. This characterization identified significant correlations between knobs and outcomes that were specific to individual inhibitors, but also were significant across all tested conditions. For example, across all conditions, the L/nL ratio is positively correlated with the cell surface hydrophobicity, and the average lipid length is positively correlated with specific growth rate. A subsequent analysis of the data with the individual inhibitors identified pairs of lipid metrics and membrane properties that were predicted to impact cell growth in seven modeled scenarios with two or more inhibitors. The L/nL ratio and the membrane hydrophobicity were predicted to impact cell growth with the highest frequency. We experimentally validated this prediction in the combined condition of 42 °C, 2.5 mM furfural and 2% v/v ethanol in minimal media. Membrane hydrophobicity was confirmed to be a significant predictor of ethanol production. This work demonstrates that membrane physical properties can be used to predict the performance of biocatalysts in single and multiple inhibitory conditions, and possibly as an engineering target. In this manner, membrane properties can possibly be used as screening or selection metrics for library- or evolution-based strain engineering.

Keywords: membrane lipid composition, L/nL ratio, membrane hydrophobicity, correlations, combined inhibitory conditions, robustness

1. INTRODUCTION

The microbial production of biorenewable fuels and chemicals requires several features to economically compete with fossil fuels (Wu et al., 2018). One such feature is the robustness of the microbial cell factory (Gong et al., 2017), where robustness describes the ability of a microbe to thrive in the desired condition, enabling bio-production at high titer, rate and yield. For example, operation at low pH and high temperature reduces the risk of contamination and reduces operating costs, but many microbial species do not tolerate these conditions. Robust biocatalysts can also tolerate lignocellulose-derived inhibitors and/or high product concentrations, increasing titers and decreasing capital costs (fermenter volume) and decreasing the operating cost of product separation. Damage to the cell membrane by these industrially appealing conditions can limit biocatalyst performance. The robustness of biocatalysts is therefore often a function of the composition and physical properties of the cell membrane.

Historically, evolution has been the main strategy for increasing tolerance. Characterization of evolved strains increases our understanding of how to achieve desired phenotypes (Portnoy et al., 2011; Zhang et al., 2009). Such characterization has identified changes to the membrane as contributing to the evolved phenotype (Cerisy et al., 2017; Chen et al., 2020; Royce et al., 2013), leading to the proposition of the cell membrane as a target for rational strain engineering (Jarboe et al., 2018; Jezierska and Van Bogaert, 2017; Liu et al., 2013; Qi et al., 2019; Sandoval and Papoutsakis, 2016). Such engineering strategies could be proposed from previous data or modeling results (Monje-Galvan, et al., 2019). Perturbation of the membrane composition and characterization of the resulting membrane properties within the design-build-test-learn cycle can also provide strategies for rational membrane engineering. Here, we have used such an approach, focusing on the membrane composition in the form of the distribution of the membrane lipids and the membrane properties of membrane permeability, membrane fluidity and membrane hydrophobicity.

Previous membrane engineering strategies have altered the membrane lipid composition via fatty acid biosynthesis enzymes, and in some cases have been successful in improving microbial growth and/or metabolic productivity. β–ketoacyl-ACP synthase I (*fabB*) modulates the abundance of unsaturated fatty acids in the *E. coli* membrane (Lennen and Pfleger, 2013; Xiao et al., 2013). Titration of *fabB* expression enabled characterization of the impact of unsaturated fatty acids on cell physiology (Budin et al., 2018). Overexpression of

β–hydroxyacyl-ACP dehydratase/isomerase (*fabA*) and the heterologous expression of fatty acid desaturase (*des*) altered the relative abundance of saturated and unsaturated fatty acids in the *E. coli* membrane and altered ethanol tolerance (Luo et al., 2009). Other heterologous enzymes, such as the cis/trans isomerase (Cti) (Tan et al., 2016)*,* and an acyl-ACP thioesterase (Lennen and Pfleger, 2013), also altered the *E. coli* membrane lipid distribution, contributing to a decrease in membrane damage and increased production of biorenewables.

In addition to the possible presence of a double bond in unsaturated membrane lipids, lipids can also be non-linear due to the presence of cyclopropane functional groups or branching. Cyclopropane fatty acids contribute to membrane stabilization, fluidity and rigidity (Grogan and Cronan, 1997; Khakbaz and Klauda, 2015; Poger and Mark, 2015) and methyl-branched fatty acids increase membrane fluidity (Poger et al., 2014). The membranes of archaeal organisms contain cyclopentane rings, increasing the temperature range over which the membrane maintains a liquid crystalline phase (Koga, 2012). This further demonstrates the concept that alteration of the distribution of the membrane lipids impacts the membrane physical properties, impacting the metabolic activity and growth of the microbial cell factory.

The membrane lipid composition can be described with various metrics, such as the relative abundance of unsaturated fatty acids and cyclic rings, the average length of the acyl chains, and the relative abundance of linear (saturated, straight-chain) and non-linear fatty acids (unsaturated or those with cyclopropane groups). For example, the metric of relative abundance of unsaturated fatty acids has been reported to vary in response to changes in temperature (Okuyama et al., 1982), pressure, abundance of ions (Mykytczuk et al., 2007), and exposure to alcohols (Luo et al., 2009) and fatty acids (Royce et al., 2013). The relative abundance of cyclic rings has been associated with tolerance of acid (Chang and Cronan, 1999; Shabala and Ross, 2008), heat, and pressure (Chen and Gänzle, 2016). Similarly, the average membrane lipid length has been reported to change in the presence of inhibitors such as short- and medium-chain fatty acids (Royce et al., 2013; Sherkhanov et al., 2014).

Given that the lipid composition of the membrane influences the membrane physical properties, fatty acid biosynthesis is crucial for membrane homeostasis (Zhang and Rock, 2008). The impact of the membrane lipid composition on the bulk cell membrane properties is demonstrated in the comparison of two familiar lipid mixtures used in cooking: fats, such as butter, and oils, such as olive oil. At ambient conditions, the higher abundance of saturated fatty

acids gives butter a relatively solid structure and less fluidity as opposed to the higher abundance of non-linear, unsaturated fatty acids and increased fluidity observed for oil.

The fact that chemical stressors can result in a change to the composition and physical properties of the membrane is well-established (Dunlop et al., 2011; Fletcher et al., 2016; Grogan and Cronan, 1997; Halverson and Firestone, 2000; Lennen and Pfleger, 2013). Ingram reported a decrease in membrane fluidity after ethanol exposure and increased fluidity after exposure to longer chain alcohols (Ingram, 1976). Besides their effect on tolerance (Luo et al., 2009; Qi et al., 2019; Wilbanks and Trinh, 2017; Zaldivar et al., 2000, 1999; Zaldivar and Ingram, 1999), and bio-production (Jiang et al., 2015; Sherkhanov et al., 2014; Tan et al., 2017b, 2016; Westbrook et al., 2018; T. Wu et al., 2018), changes to various membrane properties have been implicated in the development of other phenotypes of interest, such as biofilm formation (Zhang et al., 2007), attachment to agricultural residue (Liao et al., 2017), and antimicrobial resistance (Ghai and Ghai, 2018). These findings support the idea that membrane properties are promising targets for engineering desired phenotypes. Therefore, engineering strategies that target the membrane lipid metrics (which we view here as knobs) in order to predictably adjust the membrane physical properties (outcomes) to counteract specific inhibitory conditions could be useful for metabolic engineering applications.

As a sentinel of environmental conditions, the cell membrane both senses changing conditions and is subjected to rapid and substantial changes in its composition. These changing conditions also influence the relationship between membrane composition and membrane properties. Returning to the butter/oil analogy, these two different states of lipid bodies, butter (solid) and cooking oil (liquid), will undergo drastic changes in their physical properties within a relatively narrow temperature range; butter becomes liquid at 32 °C while oil becomes less fluid at < 4 °C. The relationship between composition and fluidity will be more difficult to detect at temperatures outside of the 4-32 °C range. Therefore, the modulation of membrane lipid composition and characterization of these membranes in a variety of conditions allows identification of relationships that can possibly be used to engineer the cell membrane to improve performance of biocatalysts (Figure 1). This approach also has the potential to guide prioritization of strains for detailed experimental characterization and could also identify cell properties that can be used as selectable indicators.

In this work, we used the FabA, FabB and Des enzymes with three different strength constitutive promoters to generate a set of strains with perturbed membrane lipid composition. These three enzymes are primarily known for their role in the biosynthesis of membrane lipids. In this framework, the range of values of membrane composition metrics are queried as knobs that possibly modulate the outputs of the membrane physical properties and microbial growth. These strains were cultured in several inhibitory conditions and a rigorous characterization of the different cell membrane response levels was performed. Systematic analysis of these data revealed membrane lipid metrics that impact membrane properties in several scenarios and in the presence of multiple inhibitors. This analysis also revealed key membrane properties that are associated with growth and production of a model biorenewable fuel in inhibitory conditions typical of industrial settings. The use of these membrane physical properties as predictors of metabolic activity can also contribute to decreasing experimental burden, and the problematic variability of strain behavior across operating scales and can serve as selection or screening markers.

2. MATERIALS AND METHODS

A brief overview of experimental procedures is provided here, with full details provided in the supplementary information. Gas chromatography-mass spectrometry (GC-MS) for the membrane lipid composition analyses, gas chromatography with a Flame Ionization Detector (GC-FID) to quantify ethanol production, and microplate reader measurements for the membrane polarization assessment were performed at the W. M. Keck Metabolomics Research Laboratory. Flow cytometry for the SYTO 9/propidium iodide viability assay was performed at the Flow Cytometry Facility at Iowa State University.

2.1 Strains, plasmids and culture conditions

E. coli strains (Table 1) were constructed by the FLP/FRT method (Datsenko and Wanner, 2000) from *E. coli* MG1655. The *des* gene was PCR amplified from *Bacillus subtilis*, which we obtained from Dr. Yandeau-Nelson's group (ISU). All primer sequences are provided in Table S1. Three distinct constitutive promoters were used: M1-12, M1-37, and M1-93, which have low, medium, and high expression strength respectively (Lu et al., 2012). Ethanol production plasmid pKS13 was previously described (Steen et al., 2010) and was obtained from Addgene (plasmid # 24627 http://n2t.net/addgene:24627; RRID: Addgene_24627).

For all cultures, single colonies were grown in 2 ml LB media for 4 h at 37 °C with rotary shaking at 250 rpm. Sixty µl of these log-phase cultures were centrifuged at 3800 g for 6 min, and cell pellets were resuspended in 3 ml MOPS containing 2% w/v dextrose at pH 7.00 (Neidhardt et al., 1974). These cultures were grown overnight (~19 h) at 37 °C 250 rpm with chloramphenicol (35 mg/L). 250-ml baffled flasks containing 25 ml minimal media MOPS 2% w/v dextrose were inoculated with overnight seed cultures to an initial $OD_{550} = 0.05$ for all tolerance experiments. The inhibitory conditions tested were 4% v/v ethanol, 0.6% v/v butanol, 0.6% v/v isobutanol, 0.1% v/v hexanol, 5 mM furfural, 100 mM acetate adjusted to pH 7.00, and the above-mentioned minimal media adjusted to an initial pH of 6.00. All cultures were maintained at 200 rpm and except for the cultures grown at 42 ºC, were grown at 37 °C. The cell densities (OD_{550}) were recorded every 2 h until the end of the log-phase. Specific growth rates were calculated during the log-phase by calculating the slope of the linearized growth rate equation $\ln(OD/OD_0) = \mu t$. Three biological replicates for each experiment generated the reported averages and standard deviations.

2.2 Ethanol production

Strains harboring pKS13 were grown for 24 h in 250-ml baffled flasks containing 25 ml minimal media MOPS 2% w/v dextrose with 5 mM furfural at 42°C with shaking at 250 rpm. Isopropyl β-D-1-thiogalactopyranoside (IPTG) at 1 mM was added for induction. Ethanol quantification was performed with Gas Chromatography with a Flame Ionization Detector (GC-FID).

2.3 Membrane characterization

Membrane characterization metrics included membrane lipid composition, fluidity, integrity, and hydrophobicity. The assessment for each membrane metric was performed in mid-log phase cultures grown in 250-ml baffled flasks containing 25 ml minimal media MOPS 2% w/v dextrose at initial pH of 7.00 (±0.02). At the time of cell harvest for the membrane characterization techniques, the pH was between 5.5 and 6.0.

2.3.1 Membrane lipid composition

Twenty-five milliliters of mid-log phase culture were harvested and subjected to lipid extraction via the Bligh and Dyer method (Bligh and Dyer, 1959), with modifications as previously described (Chen et al., 2018). Fatty acids were quantified by GC/MS using C11 and C15 saturated fatty acids as internal standards, and external standards for C16:1 and C18:1 were

assessed separately, but in the same batch of samples for analyses. Twenty micrograms of either C16:1 or C18:1 or C11/C15 were utilized for fatty acid quantification. The relative abundance of each type of fatty acid was estimated based on the total ion chromatogram peak areas relative to internal standards C11 and C15 according to their size. Specifically, C12:0 abundance was calculated with C11 internal standard, and the rest of the fatty acid abundances were calculated relative to the C15 standard. Alternatively, C16:1 and C18:1 were used as external standards, resulting in distribution estimates that were equivalent results to the use of C11 and C15 as internal standards. Representative chromatographic data is provided in the supplemental data. The relative abundance for the membrane fatty acids is presented on a mass basis.

For calculation of the L/nL ratio, the saturated fatty acids [lauric (C12), myristic (C14), palmitic (C16), and stearic (C18)] were classified as linear, while the unsaturated fatty acids palmitoleic (C16:1) and oleic (C18:1), and the cyclopropane fatty acids cycC17 and cycC19 were classified as non-linear.

$$\frac{L}{nL} = \frac{C12:0 + C14:0 + C16:0 + C18:0}{C16:1 + C18:1 + cycC17 + cycC19} = \frac{100 - \%U - \%Cyc}{\%U + \%Cyc}$$

The average lipid length was determined as previously described (Royce et al., 2013) and indicates the number of carbons in the main chain. For example, C16:0, C16:1 and C17cyc all have a length of 16.

All membrane lipid composition data, containing the abundance of each type of membrane fatty acid relative to all extracted fatty acids (%w/w), are available in supplementary information.

2.3.2 Membrane DPH Polarization

Membrane polarization was assessed utilizing the fluorescent anisotropic probe molecule 1,6- diphenyl-1,3,5-hexatriene (DPH) dissolved in dimethylformamide (DMF) (Sigma, St. Louis). This method was previously reported (Royce et al., 2013; Shinitzky and Barenholz, 1978). DPH was added to a final concentration of 0.4 µM to cells suspended in phosphate buffered saline (PBS, pH 7.00 ± 0.02) at a cell density OD_{550} ~0.1. Fluorescence polarization was measured for cells in the presence and absence of the probe molecule. The difference of fluorescence values between the treated and untreated samples was attributed to the light emitted with a degree of polarization by the excited DPH probe. A grating factor of 1.1 ± 0.1 was

estimated and used in the calculation of membrane polarization. The membrane fluidity is inversely proportional to the degree of fluorescence polarization within intact cell membranes.

2.3.3 Membrane integrity

Membrane permeability was assessed with normalized fluorescence values as described previously (Santoscoy and Jarboe, 2019) and in the supplemental methods. SYTOX Green was used at a final concentration of 5 µM. The bulk fluorescence (485/20 nm and 516/20 nm) was monitored over the growth period with one plate reader while another plate reader measured cell density (OD_{550}) in parallel. Bulk fluorescence values were then normalized by the cell density (OD_{550}).

Cell viability was determined utilizing the LIVE/DEAD BacLight Bacterial Viability Kit (Thermo Scientific, Waltham MA) containing SYTO 9 and propidium iodide (PI) fluorescent dyes. Dyes were used at a final concentration of 3.34 µM and 20 µM, respectively in 500 µl of PBS containing cells at OD_{550} 0.1. Stained cells were sorted with a BD Biosciences FACSCanto flow cytometer. This combination of SYTO 9 and PI dyes assay showed a strong correlation (R^2=0.96) with the SYTOX Green normalized fluorescence assessment (Figure S1), indicating that the membrane permeability assessment with SYTOX Green also provides estimates of cell viability.

2.3.4 Membrane hydrophobicity

Membrane hydrophobicity or microbial adhesion to hydrocarbons (MATH) was determined by measuring cell partitioning into dodecane (Sigma, St. Louis) as previously described (Pembrey et al., 1999; Rosenberg et al., 1980). Cells were suspended in PBS (pH 7.00 ± 0.02) (aqueous) at a known OD_{550}, dodecane was added to 25% v/v, and the two phases were mixed thoroughly by vortexing at 2500 rpm for 10 min. Samples were held for 15 min at room temperature to allow phase separation. The OD_{550} in the aqueous phase was re-assessed to estimate partitioning of cells into the organic phase. The percentage of cells that partitioned to the organic phase is reported as the percentage of microbial adhesion to hydrocarbons, which we use as an indicator of membrane surface hydrophobicity.

2.4 Statistics

Microsoft Office Excel was utilized for statistical analysis. T-tests were performed, and the significance level was 0.05. Data was fit to a straight line using the LINEST function. This produced a Pearson correlation coefficient (R^2), a slope, and a value for $F_{statistic}$ (F-observed).

Possible correlations for which the F value was larger than tabulated values associated with $\alpha = 0.05$ were considered to be significant. Fisher's Z values were estimated from Pearson correlation coefficients using the TANH function (Alexander, 1990).

Significance of the differences between the experimental and the predicted normalized membrane metrics was assessed by comparison to a random sampling of 100 values ranging from 0 to 1. This randomly-generated population was converted to a standard normal distribution. The absolute values of the differences between the normalized predicted value and the normalized experimental data were converted into Z-score values. These Z-scores were interpolated from Z-charts ($\alpha=0.05$) to find the corresponding area under the curve, which was then used to calculate p-values from the normal standard distribution.

2.5 Prediction of correlations in theoretical combined conditions

Experimentally-derived Pearson correlation coefficients from individual inhibitor experiments were used to estimate correlation coefficients for theoretical conditions with multiple inhibitors. Experimental correlation coefficients were transformed into Fisher's Z values, enabling the averaging of these values across each of the inhibitors involved in each theoretical scenario. Then, the calculated average Z-values were re-transformed into combined correlation coefficients (Alexander, 1990). Sixty-two combined inhibitory scenarios were chosen considering the potential combinations of: one product (ethanol, butanol, isobutanol or hexanol); one or more lignocellulosic-derived inhibitors (furfural and/or acetate); and one or more physical inhibitory conditions (42 ° C and/or pH 6.00). For each scenario, we used the magnitude of the combined correlation coefficients to propose the outcome (membrane property or growth) that is the most strongly correlated with one of the lipid knobs. We similarly propose for each condition the membrane lipid metric (level 2) or membrane property (level 3) that is the most strongly correlated to growth (level 4). For each calculated combined correlation coefficient, we also calculated a standard deviation.

The Excel file utilized for the preparation of Table 2 showing this analysis is available in supplementary information.

2.6 Graphics

Illustrations were created with Biorender.com and GraphPad Prism 8.

3. RESULTS AND DISCUSSION

3.1 Perturbation of membrane lipid composition

We perturbed the membrane lipid composition by targeting the relative abundance of unsaturated fatty acids via the Des, FabB and FabA enzymes. Similar alteration of the membrane lipid composition in *E. coli* has been previously demonstrated by the overexpression of *fabA* and the heterologous expression of the *B. subtilis des* gene (Luo et al., 2009). In this previous work, the *+fabA* strain had a higher relative abundance of saturated fatty acids and increased ethanol tolerance than the control strain. In contrast, expression of *des* was associated with increased abundance of unsaturated fatty acids and increased ethanol sensitivity. Our other engineering target, *fabB*, has previously been reported to change the relative abundance of saturated and unsaturated fatty acids (Xiao et al., 2013). Thus, we used these three engineering targets to generate a set of *E. coli* strains with perturbed lipid composition, with the goal of using this set of strains to identify correlations between membrane composition, membrane properties, and microbial metabolic activity in the form of growth. These strains differed in the identity of the target enzyme (FabA, FabB, Des) and the strength of the associated promoter (Table 1). We quantified the resulting membrane composition in this set of ten strains in our baseline growth condition of MOPS 2% w/v dextrose at 37 °C, with an initial pH of 7.00 (±0.02).

We observed both a significant increase and a significant decrease in the percentage of unsaturated fatty acids among these strains. The strain with the most moderate promoter (M1-12) for *fabA* (fabA12) had a significant decrease in the relative abundance of unsaturated fatty acids compared to the control (Fig. 2A). Likewise, the levels of unsaturated fatty acids increased the most when the *des* gene was expressed with the highest strength promoter. In this way, we were able to modulate the percentage of unsaturation from 1.4 ± 0.2 (fabA12) to 20.4 ± 0.3 (des93) in the baseline condition. These results are consistent with previous reports for strains expressing *des* and *fabA* (Luo et al., 2009). FabB was previously found to be crucial for directing the metabolic flux of fatty acid biosynthesis towards unsaturated fatty acids rather than saturated (Xiao et al., 2013), consistent with our observation of an increase in the percentage of unsaturated fatty acids proportional with the strength of the promoter driving *fabB* expression.

A previous characterization of deletion mutants of *fabA* or *fabB* indicates that *E. coli* requires a minimum of 15% unsaturated fatty acids for growth at 37 °C (Cronan et al., 1969) (Cronan and Gelmann, 1973), but other reports have described *E. coli* strains containing less than 15% unsaturated fatty acids (Budin et al., 2018; Yuk and Marshall, 2005). The relatively low

abundance of unsaturated fatty acids in our control strain (5%) appears to be related to our choice of baseline condition, as we observed 18% unsaturation in this strain when grown in rich media (Figure S2). We did note that within our set of strains, the combined relative abundance of unsaturated and cyclopropane fatty acids is always at least 17% across all culture conditions.

The Des enzyme has been reported to introduce unsaturation at different positions of the fatty acid depending on the culture conditions (Bonamore et al., 2006), including production of C16:1 Δ5 (Luo et al., 2009). However, C16:1 Δ5 and C16:1 Δ9 were not resolved in the analytical methods used here and our analysis does not distinguish between these two isomers.

While it was expected that our selected engineering targets of FabA, FabB and Des would primarily result in perturbation of the abundance of unsaturated fatty acids, changes were also observed for the average lipid length, the relative abundance of cyclic rings, and the ratio of linear relative to non-linear fatty acids (Figure 2). Our engineered strains showed both a decrease and an increase in the average lipid length relative to the control, ranging from 15.78 (fabA12) to 16.07 (fabB93). Strains engineered for expression of FabB or Des showed an increase in the average lipid length relative to the control. Surprisingly, +fabA strains showed both a significant decrease (fabA12) and a significant increase (fabA93) in average lipid length. The relative abundance of cyclic rings is known to increase when cells enter stationary phase (Wang and Cronan, 1994) and thus we restricted our sampling to the mid-log phase. The relative abundance of cyclic rings varied from 14% (des93) to 20% (several strains), although none of the strains showed a significant increase in cyclic rings relative to the control in the baseline condition.

Previous reports of expression FabA and Des from plasmids at a single induction level in *E. coli* strain W3110 in rich media described lipid length values of 15.75 - 15.92, and cyclic ring abundances of 3.5 - 6.4% (Luo et al., 2009). Thus, we obtained a larger range of values for both of these lipid metrics compared to this previous study. The abundance of cyclic rings decreased relative to the wild-type strain for most of our engineered strains, similar to Luo's study. The smaller lipid length of fabA12 (15.78) relative to the control (15.92) is also consistent with the previous study's report of the strain engineered for increased *fabA* expression having a shorter average lipid length (15.75) relative to the control strain (15.92). In addition, the previously reported lipid length of the *fabA*-expressing strain was smaller than *des*-expressing strain (15.89) and this was also generally observed for our set of MG1655-derived strains expressing Des and FabA.

Our final metric is the ratio of linear-chain (saturated) fatty acids relative to the non-linear (unsaturated or with a cyclic ring). This metric considers the poor stacking that both unsaturated and cyclopropane fatty acids have in the cell membrane as a consequence of their conformation. Strains with higher L/nL ratio values contain a larger amount of saturated or 3D-spatially stable fatty acids relative to the more dynamic and bent type of fatty acids. Values of this lipid metric ranged from 1.90 (des93) to 4.85 (fabA12) in the baseline condition.

These results demonstrate significant variation in each of the four lipid composition metrics (level 2 knobs) during growth in the baseline condition for this set of strains. For the percentage of unsaturated fatty acids, the average lipid length, and the L/nL ratio, values were both greater than and lower than the values for the control strain and the observed variation corresponded to the strength of the utilized promoter.

3.2 Modulation of membrane lipid metrics impacts membrane properties and growth

Having observed significant variation in membrane composition in the set of engineered strains, we next quantified changes in membrane physical properties (Figure S4). Membrane damage is often quantified in the form of cell membrane permeability, due to the inability of some fluorescent probes to cross intact membranes. Membrane fluidity is a function of flexible components, such as the unsaturated fatty acids, and this dynamic environment can be assessed by the movement of anisotropic fluorescent probe molecules, such as DPH (Royce et al., 2013; Shinitzky and Barenholz, 1978). The membrane hydrophobicity quantifies the partitioning of the microbe into a hydrocarbon, such as dodecane, relative to an aqueous solution. Similar to the membrane fluidity, hydrophobicity is a function of multiple membrane components. Together, these properties provide the opportunity to quantify distinct physical alterations of the cell membrane.

The majority of our strains had significantly altered membrane hydrophobicity and permeability (Figure S4). The strains fabB37 and fabA37 had significantly increased membrane hydrophobicity relative to the control strain while all three strains expressing the *des* gene had lower values of this metric relative to the control strain. This indicates that the different membrane lipid composition of these strains impacted the microbial surface hydrophobicity, as demonstrated by the partitioning of cells into the organic phase. None of the engineered strains showed increased membrane integrity relative to the control, meaning that they did not show decreased permeability to the SYTOX nucleic acid dye. Interestingly, the permeability of strains

fabB12 and fabB37 increased by two orders of magnitude relative to the control. However, these two strains did not show atypical values of the four membrane lipid composition metrics (Figure 2). The strain des93, with the highest abundance of unsaturated fatty acids, had an unexpected decrease in membrane fluidity, as evidenced by an increase in DPH polarization (Figure 2A, Figure S4B). This demonstrates that membrane functionality depends on more than one lipid metric and demonstrates the need for rigorous characterization across multiple metrics.

We envision the membrane lipid metrics as different knobs that can be adjusted in order to modulate values in the corresponding outcomes of membrane physical properties and, ultimately, metabolic activity and growth. Consistent with this model, modulation of membrane lipid compositions in our set of engineered strains had different outcomes in terms of membrane functionalities and cell growth in the baseline condition, enabling identification of significant correlations (Figure 3A).

For example, the L/nL ratio and the lipid length are significantly correlated ($p<0.05$), such that as L/nL increases, the average lipid length decreases (Figure 3B). Consistently across our set of strains, the average length of saturated fatty acids was shorter (15.85 ± 0.05) than the average length of unsaturated fatty acids (16.74 ± 0.26) and fatty acids containing cyclic rings (16.05 ± 0.04). The percentage of unsaturated fatty acids was the largest for des93 ($20.4\% \pm 0.3$) and the lowest for fabA12 ($3.7\% \pm 0.7$), and these two strains had the second largest and the smallest lipid length values (16.07 ± 0.00 and 15.78 ± 0.00, respectively) (Figure 2A, 2B). The L/nL ratio deviated from -35% (des93) up to +63% (fabA12) of the value for the control strain.

In the baseline condition, significant correlations were also observed between the percentage of unsaturated fatty acids and both the average lipid length and the L/nL ratio. The form of the equation for the L/nL ratio imposes an inverse relationship between L/nL and the relative abundance of both unsaturated fatty acids and cyclic rings, though the magnitude of this connection in the various conditions is not subjected to a fixed mathematical constraint. The framework demonstrated here for identifying relationships between membrane metrics in the baseline condition indicate that this type of analysis could be performed on a variety of inhibitory conditions of interest.

3.3 Engineering of the membrane lipid composition impacts tolerance of some membrane-damaging conditions

It has been widely demonstrated that changes to the membrane composition can impact tolerance of membrane-damaging compounds (Chen et al., 2018; Luo et al., 2009; Qi et al., 2019; Royce et al., 2013; Sherkhanov et al., 2014; Tan et al., 2016; Westbrook et al., 2018; Wikström et al., 2009; Wilbanks and Trinh, 2017). Therefore, we tested the tolerance of our set of strains in the baseline condition of MOPS 2% w/v dextrose modified to contain either 5 mM furfural, 100 mM acetate adjusted to pH 7.00, 4% v/v ethanol, 0.6% v/v butanol, 0.6% v/v isobutanol or 0.1% v/v hexanol. These chosen concentrations each caused a $50 \pm 10\%$ decrease in specific growth rate relative to the baseline condition for the control strain. We also characterized growth of these strains when cultured in the baseline condition modified to a temperature increase to 42 °C or adjusted to pH 6.00. The set of strains showed significant changes in the specific growth rate relative to the control strain in all tested inhibitory conditions except for isobutanol and hexanol (Figure 4).

The most considerable changes in tolerance among these strains were observed for furfural and for high temperature. The strain fabA37 had a 30% increase in growth rate relative to the control strain in both of these conditions. This increase in growth rate was the highest compared to other strains and other inhibitory conditions. Several strains had increased tolerance for higher temperature or furfural conditions except in a few cases where the weakest promoter was utilized. Specifically, the M1-12 promoter in front of *des* or *fabB* genes did not increase thermotolerance, and when this promoter was used to regulate *fabA*, there was also no change in furfural tolerance. The rest of the engineered strains with the higher strength promoters showed increased tolerance to both the increased temperature and furfural culture conditions.

In contrast to the substantial number of strains with increased tolerance to 42 °C or furfural challenge, only a few strains showed significant changes in specific growth rate when grown in the presence of ethanol or butanol. The three strains expressing the Des enzyme, as well as the fabB12 and fabB37 strains, actually showed increased sensitivity to ethanol, as evidenced by a specific growth rate significantly lower than the control strain. The fact that no strains showed changes in specific growth rate during challenge with isobutanol or hexanol implies that the range of membrane lipid compositions sampled here did not benefit the organisms during challenge with these alcohols. This in turn suggests that either mechanisms of toxicity distinct from membrane damage are responsible for the observed inhibition or that the modulation of lipid content in our engineered strains is insufficient to alter growth.

16

It was previously reported that tolerance to ethanol corresponds to increased levels of saturated fatty acids while ethanol sensitivity is associated with unsaturated fatty acids (Luo et al., 2009). Another study attributed ethanol, butanol and isobutanol toxicity to mechanisms besides membrane fluidity and integrity (Huffer et al., 2011). This prior study did not observe significant correlations between the shifts of fatty acid composition and membrane fluidity or tolerance. The fact that previous investigations were able to link membrane composition and tolerance of ethanol but not tolerance of butanol and isobutanol is consistent with different length carbon-chain alcohols impacting the cell membrane differently. The toxicity of alcohols is known to be directly related to the carbon length (Mukhopadhyay, 2015). Toxicity studies towards four- and five-carbon alcohols have reported evidence of membrane alterations and membrane related genes for alcohol tolerance regardless of their length (Foo et al., 2014; Minty et al., 2011; Reyes et al., 2011; Rutherford et al., 2010). This suggests that further modulation of membrane elements might produce tolerance towards diverse alcohols.

3.4 Microbial inhibitors caused different changes in membrane metrics of the control strain

As expected, the composition and properties of the cell membrane of the control strain differed in the various inhibitory conditions (Table S2). The greatest observed change of membrane lipid composition metrics in the control strain relative to the baseline condition was a 6-fold increase in the percentage of unsaturated fatty acids in the presence of hexanol. Other changes include a 2.3-fold decrease in the membrane hydrophobicity during growth in the presence of butanol and increased membrane permeability during growth at 42 °C (3.8-fold) or with hexanol (2.27-fold).

These observed changes in composition and properties of the cell membrane demonstrate the diversity of cell membrane responses to various stimuli. The set of engineered strains with modulated membrane lipid composition provided us with the opportunity to perform a thorough characterization of membrane metrics in various conditions and identify the relationship between the different cell membrane response levels for each inhibitory condition.

3.5 Set of engineered strains had inhibitor-dependent range of values of membrane metrics

Our alteration of the membrane composition is expected to impact the outcomes of exposure to different inhibitory conditions. This expectation is supported by the differing

outputs, in terms of specific growth rate of the biocatalyst, in the presence of these stressors (Figure 4). Characterization of the membrane composition and properties for the set of engineered strains in the eight inhibitory conditions provides data for mapping the connections between lipid composition and membrane properties (Figure 5, Figure S5).

The membrane metrics of each strain can be assessed as part of a range of values for the entire set of strains. As expected, these strains showed inhibitor-dependent differences in the membrane lipid metrics and membrane properties relative to the baseline condition. For example, when cells were grown in the presence of acetate, the percent of unsaturated fatty acids ranged from 2% (fabA93) to 12% (des93), but in the presence of hexanol the percent of unsaturated fatty acids ranged from 29% (fabB12) to 40% (des93).

Some strains demonstrated consistent trends across conditions. The strain des93 had an increase in the relative abundance of unsaturated fatty acids relative to the control strain in all conditions (Figure 5A), consistent with the known desaturase activity of Des. This strain had the lowest abundance of cyclic rings in the baseline condition and values below the second quartile across all microbial inhibitors except for furfural. The use of the weakest promoter (M1-12) with fabA resulted in the lowest percentage of unsaturated fatty acids and shortest lipid length in the baseline condition. For the other FabA strains, the values of these two metrics were below the second quartile across most conditions. In contrast to the fabA strains having a relatively low percentage of unsaturated fatty acids and relatively short lipid length, these strains also appeared in the upper third quartile of membrane hydrophobicity values for all conditions except for butanol and isobutanol. Another trend observed in all conditions is the dramatic increase in membrane permeability by fabB12 and fabB37 relative to the control strain (Figure S7-A). In general, other than the examples described above, most engineered strains showed both an increase and a decrease relative to the control strain for all lipid metrics and membrane properties, depending on the inhibitory condition. This demonstrates the need for identifying the most tunable membrane metric in a specific condition and designing a membrane engineering strategy to reach the desired results.

The growth conditions with the largest range of the percentage of unsaturated fatty acids relative to the baseline condition were furfural and isobutanol (Figure 5A). These large ranges demonstrate our ability to sample extreme values of these metrics. The range of values for average lipid length also changed in an inhibitor-dependent manner although these ranges were

not as large compared to those observed for the percentage of unsaturated fatty acids. Surprisingly, there was a general increase of lipid length for all of the inhibitory conditions relative to the baseline condition (Figure 5B).

Similarly, the abundance of cyclic rings varied greatly depending on the growth condition. Cultures in the baseline condition that showed an overall abundance of cyclic rings up to 20% had a 2-fold increase and decrease in the maximum average abundance of cyclic rings when the culture conditions were acetate or hexanol, respectively (Figure 5C). Some stressors had a uniform impact on cyclic ring abundance, meaning that for all ten strains the abundance of cyclic rings either increased (pH 6) or decreased (ethanol, butanol and hexanol) relative to the baseline condition (Figure 5C). Across all strains, the range of cyclic ring abundance during growth with furfural ranged from 5 – 29%, the largest range observed among the growth conditions.

Given the observed changes in the relative abundance of unsaturated fatty acids and cyclic rings, it is not surprising that the L/nL ratio also displayed substantial variation. Ethanol cultures had L/nL ratio values ranging from 2.3 to 8.6 (Figure 5D). Ethanol was previously reported to increase the relative abundance of saturated fatty acids (linear) in the cell membrane of other bacteria (Grandvalet et al., 2008), and this might occur as a compensation for the increase in membrane fluidity (Dombek and Ingram, 1984).

Among the membrane physical properties, membrane hydrophobicity had the largest change across the culture conditions (Figure 5E). This demonstrates that the set of engineered strains not only produced a range of values for membrane lipid metrics but also that these changes were associated with changes to other measurable bulk membrane features. Cells grown at 42 ℃ showed the largest range of hydrophobicity values, ranging from 9% to 83%. In contrast, in the baseline condition the hydrophobicity values ranged only from 4% to 46%. This supports the drastic effect that temperature can have on membrane properties (Shirley et al., 1987; Szekely et al., 2011). In addition to the variation of membrane hydrophobicity at the higher temperature, hexanol had a shorter range of hydrophobicity values relative to the other shorter chain alcohols. Notably, the strain fabB12 had a dramatically increased membrane hydrophobicity (~ 80%) only when exposed to four-carbon alcohols. Our data and previous studies indicate that membrane hydrophobicity is a responsive physical property to various type of stimuli.

19

For the membrane polarization values, all inhibitory conditions, except for hexanol and pH 6, showed similar range (Figure 5F). Hexanol cultures had a substantial increase in membrane fluidity, as evidenced by a decrease in polarization, compared to shorter carbon length alcohols, which is consistent with previous reports (Dombek and Ingram, 1984).

Similar to the observations for membrane hydrophobicity, the values for membrane permeability had the largest magnitude and the largest spread during growth in minimal media at 42 ℃ (Figure 5G). In agreement with our data, membrane leakage after furfural exposure was reported to not change significantly in *E. coli* (Mills et al., 2009). In contrast, we observed that alcohols increased membrane leakage for all strains. For the shortest alcohol, ethanol, the overall membrane permeability values increased, consistent with previous knowledge of ethanol exposure and increased membrane leakage (Eaton et al., 1982) and fluidity (Dombek and Ingram, 1984). Even though toxicity associated with longer chain alcohols might rely on multiple mechanisms besides the effects on the cell membrane, our data, as well as previous reports (Foo et al., 2014; Minty et al., 2011; Mukhopadhyay, 2015; Reyes et al., 2011; Rutherford et al., 2010), indicate that these alcohols impose various effects on the cell membrane. This set of engineered strains with perturbed lipid composition sheds light on the effects of diverse stressors on the cell membrane aside from specific growth rate.

3.6 Membrane metrics show stress-specific correlations between response levels

We performed a systematic statistical analysis of non-random regressions in order to assess potential connections between the system knobs (membrane lipid parameters) and their outcomes (membrane properties and cell growth). This analysis utilized the data from of all tested individual stressors. The significant connections are depicted in a general stress-response network (Figure 6-I).

This lumped analysis shows that across conditions, the L/nL ratio has a significant inverse association with each of the other three membrane lipid metrics. The inverse relationship between the L/nL ratio and the relative abundance of unsaturated and cyclic lipids was expected based on the structure of the L/nL calculation. However, the association of the L/nL ratio and average lipid length is not mathematically constrained. Given that design engineering strategies likely alter additional membrane metrics, the L/nL ratio appears to be a meaningful knob for modifying and evaluating the membrane lipid composition of cells when exposed to stress. The

20

stress-response network for the combined individual inhibitory conditions also suggests that the L/nL ratio and average lipid length can be used as knobs for modulating the outcomes of membrane hydrophobicity and cell growth, respectively.

An inhibitor-specific response network was similarly produced utilizing the data from each individual inhibitory condition (Figure 6-II, III). A variety of growth inhibitors such as acetate, pH 6, ethanol and isobutanol demonstrated a correlation between the L/nL ratio and the relative abundance of cyclic rings. The L/nL ratio also was correlated to the three membrane physical properties in several distinct conditions. Specifically, the L/nL knob influenced the membrane hydrophobicity in the conditions of 42 °C, furfural or ethanol. The membrane hydrophobicity also showed a connection with growth in the presence of butanol. Cultures at higher temperatures are advantageous in industrial fermentations for reducing contamination and cooling costs (Caspeta et al., 2014; Curran et al., 1989).Going back to the example of butter and olive oil, we observed that the L/nL ratio was significantly related to the membrane polarization, with cells grown at 42 °C having a decreased L/nL ratio and a corresponding decrease in DPH polarization ($R^2 = 0.64$), indicative of increased fluidity (Figure 6-IIIA). Among the various inhibitory conditions, this relationship was observed only at 42 °C, demonstrating that manipulation of the L/nL ratio is not a universally effective knob when attempting to tune the membrane polarization.

Furfural and acetate are often present in depolymerized lignocellulosic biomass (Chi et al., 2019; Ding et al., 2011; Zhao et al., 2015). We observed that in the presence of furfural, the L/nL ratio showed a significant correlation with membrane hydrophobicity ($R^2 = 0.58$). In contrast, the modulation of average lipid length showed an inverse relationship with hydrophobicity ($R^2 = -0.16$). The observed relationship between average lipid length and growth in the presence of furfural ($R^2 = 0.55$) is particularly promising and demonstrates the utility of employing other knobs besides the L/nL ratio.

Growth in the presence of acetate produced the highest number of significant correlations between membrane metrics, consistent with the fact that many of the known acetate toxicity mechanisms are associated with the cell membrane (Trček et al., 2015). Within our set of strains, the relative abundance of cyclic rings during growth in the presence of acetate significantly correlated with each of the other three membrane lipid metrics. Specifically, cyclic ring abundance correlated with unsaturated fatty acids relative abundance ($R^2 = -0.76$), average lipid

length ($R^2 = -0.64$), and the L/nL ratio ($R^2 = -0.92$), where the negative relationship here is expected due to the structure of the L/nL calculation. Cyclic rings also had influence on the membrane physical property of polarization ($R^2 = -0.59$). Also, in the presence of acetate we observed correlation between the percentage of unsaturated fatty acids and polarization ($R^2 = 0.87$), and between the L/nL ratio and membrane permeability ($R^2 = 0.74$), respectively. These results show the different levels of cell membrane response caused by acetate and the complexity of these effects on the membrane properties.

When cells were grown in the presence of ethanol, the largest range of L/nL ratios was observed and these values significantly correlated with membrane hydrophobicity ($R^2 = 0.61$) (Figure 6-IIIE). We also observed a significant relationship between membrane polarization and permeability in this condition.

Butanol and isobutanol are isomers with different membrane effects (Huffer et al., 2011) therefore membrane design strategies should consider these differences. In the presence of isobutanol, there were no significant correlations observed for membrane properties or growth, all significant correlations were between lipid metrics. Contrastingly, for butanol, significant correlations were observed between hydrophobicity and: polarization, permeability and growth (Figure 6-IIIF,G). This difference suggests that butanol has an effect on non-lipidic elements of the cell membrane not quantified here. Such non-lipidic elements could be phospholipid head groups, peripheral and transmembrane proteins, and/or the polymeric matrix. These results also suggest that membrane engineering strategies that target hydrophobicity could be effective for improving the performance of butanol producers, but not isobutanol producers. These differing results highlight the need for careful consideration of the condition of interest when designing a membrane engineering strategy.

Membrane hydrophobicity was the outcome that showed the most connections with either lipid metrics or with other physical membrane properties, including all tested straight-chain alcohols (Figure 6-III). Interestingly, hydrophobicity and polarization were significantly correlated in the presence of both butanol and hexanol, but in opposite directions ($R^2 = -0.55$ and 0.62, respectively). Together, these data further emphasize that membrane hydrophobicity is a critical membrane property, and that the L/nL ratio, and possibly to a lesser degree the average lipid length, are knobs that can be adjusted in order to tune this property. This again

demonstrates that the design of membrane engineering strategies needs to be carefully tailored to the condition of interest.

The absence of significant correlations in some conditions can challenge current notions about the effect of some stressors on the cell membrane. For example, the L/nL ratio should be inversely related to both the relative abundance of unsaturated lipids and cyclic lipids. However, this effect was dominated entirely by either cyclic lipids in some conditions or by unsaturated lipids in others (Figure 6-III).

E. coli exposure to acidic media has been associated with increased expression of membrane-related genes, such as cyclopropane fatty acid synthase (Chang and Cronan, 1999). While acidification of the media (pH 6.00) had the expected impact on cyclic fatty acid content, we did not detect any correlations between this altered membrane lipid composition and the membrane physical properties (Figure 6-IIIH). This lack of changes indicates either that the membrane properties are relatively robust in this condition, or that alternative membrane targets besides membrane lipid composition should be used to tune acid tolerance. The fact that the global regulator RpoS has been previously implicated in the acid response (Chang and Cronan, 1999) is consistent with mechanisms of inhibition distinct from the cell membrane.

The analysis presented here focuses on characterization during mid-log growth. However, our method for tracking membrane permeability tracks the entire growth period (Figure S7) and membrane permeability has been previously reported to spike during lag phase, as cells adapt to the new culture media (Rolfe et al., 2012; Santoscoy and Jarboe, 2019). Acid tolerance is also known to depend on the adaptation of the cells to acidic environments during lag phase (Šeputienė et al., 2006). Consistent with previous reports, all of our strains in all of the culture conditions had higher membrane permeability during lag-phase relative to mid-log growth (Figure S7). The magnitude of this difference was notably smaller for the 42 °C condition relative to the other conditions.

Membrane permeability is a classical membrane metric for development of robust microbial cell factories, largely due to the ease of measurement, and this property was reported to be related to tolerance and production of fatty acids (Santoscoy and Jarboe, 2019; Tan et al., 2017a). However, membrane integrity did not correlate with growth in any of the inhibitory conditions, and we only observed a significant association of membrane lipid composition with membrane permeability during growth in the presence of acetate (Figure 6-IIIC). This is

consistent with the idea that membrane integrity is a function of additional membrane components, not just the lipid distribution. For example, specific lipoproteins were reported as essential to maintenance of membrane integrity across organisms (Kaplan et al., 2018; Ryan et al., 2010; Xie et al., 2016).

Together these data demonstrate that perturbation of the fatty acids in the cell membrane had a different impact on membrane properties in different conditions. We identified correlations in each individual inhibitory condition and found that, in general, the L/nL ratio was the most predominant knob, impacting each of the three membrane physical properties, and the membrane hydrophobicity was the most frequently impacted outcome.

3.7 Systematic analysis enabled identification of membrane metrics to predict cell growth in combined inhibitory conditions

Our perturbation of membrane lipid metrics enabled identification of connections with membrane properties across a spectrum of individual inhibitory conditions, demonstrating the specificity of some of these connections to the relevant inhibitor. However, it is not clear how these inhibitor-specific connections interact in the presence of multiple inhibitors. It becomes increasingly resource-intensive to thoroughly characterize a set of strains across multiple combinations of inhibitors. Thus, it is desirable to use the single-condition data to predict the potential outcomes in the presence of multiple inhibitors, with the goal of down-selecting strains for experimental characterization.

We used our systematic analysis of individual inhibitory conditions, membrane composition, properties, and growth to predict which knob/outcome connections are most active and are connected to microbial growth across 62 theoretical scenarios involving combinations of the individually characterized inhibitors (Figure 6). This prediction was based on summation of the Pearson correlation coefficients (Alexander, 1990). For each scenario, we identified the outcome (membrane property or specific growth rate) that is the most strongly correlated with one of the lipid knobs. We also identified the membrane lipid metric (level 2) or membrane property (level 3) that is the most strongly correlated to growth (level 4).

This analysis led to the identification of clear design strategies for some conditions, but not others (Table S3). We down-selected the model results to those that show a continuity across lipid metric, membrane property and growth and based on the confidence interval of the

predicted correlation coefficient (Table 2). For five of these seven scenarios, some lipid knob (level 2) is predicted to be significantly correlated with a membrane property (level 3) and that same membrane property is predicted to be significantly correlated with growth rate (level 4). In all of these five cases, the membrane property is hydrophobicity, and it should be noted that each of these five scenarios involves elevated temperature as one of the stressors. For the other two scenarios, a lipid knob (specifically, average lipid length) is significantly correlated with both a membrane property and growth.

3.8 Membrane properties in combined conditions can be predicted from lipid metrics

For experimental validation of these predictions, we chose the triple scenario with higher temperature (42 ℃) in the presence of furfural and ethanol. This theoretical scenario had moderately high combined correlation coefficients for the L/nL ratio modulating membrane hydrophobicity, with membrane hydrophobicity in turn modulating growth rate (Table 2). We also chose to partially characterize the scenario with acetate and hexanol because it had the highest combined correlation coefficient (0.70) of lipid metrics, specifically average lipid length, modulating a membrane physical property, specifically membrane hydrophobicity, across all hypothetical scenarios (Table S3). Note that in this scenario hydrophobicity was not predicted to impact growth and thus it is not listed in Table 2. The full results of these experiments are provided in supplementary information (Figure S9). We observed that the predicted lipid metrics (knobs) were efficacious predictors of the membrane properties (outcomes) for the two selected combined scenarios.

Experimental measurements of the membrane hydrophobicities in these two multi-stressor conditions were found to more strongly correlate with the values of the corresponding lipid knobs than to the membrane hydrophobicities from the single-inhibitor experiments. In the triple condition with ethanol, furfural and elevated temperature, the sum of squared errors (SSE) when the L/nL ratio was utilized as predictor of the membrane hydrophobicity, was lower than the SSE from using the single-condition hydrophobicity values. Similarly, the average lipid length was a better predictor of membrane hydrophobicity in the presence of acetate and hexanol. Thus, in both of these scenarios, the use of the lipid metric knob to predict the hydrophobicity in the multi-stressor condition was better than the use of the hydrophobicity in the single inhibitor condition.

We also compared the performance of these lipid knobs to a series of sham randomized metrics and determined that our use of the individual L/nL values to predict the membrane hydrophobicity in the triple scenario had a significantly lower average absolute difference than this random population ($p = 0.031$). For the acetate/hexanol condition, the use of the lipid length as the predictor was not significantly better than the random predictions ($p = 0.4$).

These results highlight the relevance of using a systematic approach to identify lipid metrics that correspond to specific membrane properties. This identification of a knob-outcome connection can be utilized in strain design and can guide the prioritization of strains for experimental characterization, possibly increasing the efficiency of the build-test-learn component of the design-build-test-learn cycle.

3.9 Biocatalyst performance can be predicted from membrane properties

The results above demonstrate that lipid characteristics (level 2) measured in the presence of individual stressors significantly correlate with membrane properties (level 3) in the presence of a combination of those stressors. Ultimately, the goal here is to identify membrane metrics that can be used as engineering targets to improve microbial robustness in the form of microbial growth and/or metabolite production (level 4).

The systematic framework demonstrated here predicts that hydrophobicity is an alternative metric for metabolic activity, in the form of specific growth rate, in the triple condition of $42^{\circ}C$, ethanol and furfural (Table 2). We experimentally measured the growth rate in the triple inhibitor scenario and verified its significant correlation with the membrane hydrophobicity ($R^2 = 0.47$, $p<0.05$) (Figure 7A). The metabolic activity was also assessed in the form of ethanol production in minimal media with furfural at $42\ ^{\circ}C$. Ethanol titers were observed to significantly correlate with membrane hydrophobicity ($R^2 = 0.43$, $p<0.05$, SSE=0.72) but not with specific growth rate (Figure 7C). Other metrics to determine robustness, such as cell viability determined by fluorescent dyes did not correlate either to ethanol productivity or to membrane hydrophobicity (Figure S10). Thus, screening the library on the basis of growth with the goal of down-selecting for ethanol production would not be successful, but screening the library on the basis of hydrophobicity would. These results show the success of this experimental framework.

3.10 Potential Applications

Implementation of metabolic engineering strategies often involves the construction of a strain library, where this library either consists of multiple distinct genetically homogenous strains or is a heterogenous mixture, such as genome-scale libraries. Screening of either type of library directly for metabolite production can be challenging and resource intensive. Growth is often used as a proxy of metabolic activity, particularly in the context of maintenance of redox balance or ATP production. For example, a library of 243 strains engineered for isobutanol production were down-selected on the basis of colony size (Ghosh et al., 2019). Other strategies for reducing the experimental burden in library down-selection include statistically guided sub-sampling (Young et al., 2018), and use of colorimetric assays, often involving biosensors (Scheel and Lütke-Eversloh, 2013).

Membrane properties may be linked to metabolic activity and could be more readily measured or assessed than metabolite productivity. The straightforward nature and accessibility of the hydrophobicity and permeability assays are especially appealing, and both of these assays could be used as selection methods for a heterogenous population, similar to the enrichment of lipid-producing strains based on their propensity for floating (Liu et al., 2015).

The calculation of growth rate for multiple strains and conditions is manageable at small scale with high-throughput capabilities, but these growth rates often do not correspond to larger scales (Wehrs et al., 2019) and estimation of the growth rate and identification of the most robust strains at larger scales can be more resource intensive. Thus, the identification of microbial properties other than growth that are related to metabolic activity provide an alternative metric that may be more robust across conditions, in terms of media composition and working volume. Also, some research groups do not have the capacity, either at the level of researcher time/effort and/or funding to support comprehensive tracking of metabolite productivity for a large library. Identification of alternative metrics associated with metabolite productivity can possibly be beneficial in reducing the experimental burden. Assessment of membrane properties, such as hydrophobicity, can often be performed with a single sampling of mid-log growth, as opposed to the multiple samplings needed for estimates of metabolite productivity or growth rate. Together these data highlight the relevance of assessing and identifying impactful membrane physical properties to predict metabolic activity and cell performance. We envision that rigorous experimental characterization of membrane metrics, and a systematic approach for data analysis

can contribute to identification of membrane physical properties that can be used as either engineering targets or as markers for selection or screening.

4. CONCLUDING REMARKS

Biocatalysts are exposed to a plethora of stimuli that perturb the cell membrane. The self-regulating mechanisms that cells use to survive in harsh conditions can be viewed as a response network of knobs and outcomes, culminating in the metabolic activity of the organism, demonstrated with growth and metabolite production. The network that governs this regulation is an attractive tool for incorporation into the design-build-test-learn metabolic engineering cycle, but such use of this network requires knowledge of its structure.

The use of different promoters to drive expression of *des*, *fabA* and *fabB* resulted in a set of strains with altered membrane fatty acid compositions. The percentage of unsaturation, abundance of cyclic rings, lipid length, and L/nL ratio were used as metrics to quantify the membrane lipid composition and these cells were characterized in terms of their membrane hydrophobicity, fluidity (DPH polarization) and integrity (permeability).

Exposure of this set of strains to various inhibitory conditions and the rigorous experimental characterization of their membrane metrics produced inhibitor-dependent ranges of values for each membrane metric (Figure 5). We employed a systematic approach for mapping the response network of knobs and outcomes for individual inhibitors (Figure 6). This analysis enabled the prediction of lipid metrics that could be utilized as knobs to modulate specific outcomes (*i.e.,* membrane properties and cell growth) in 62 theoretical scenarios with two or more stressors (Table S3).

The experimental validation of this approach in the triple condition of minimal media at 42 °C, furfural and ethanol showed that the newly defined ratio of linear to non-linear fatty acids (L/nL ratio) predicted the experimental membrane hydrophobicity (Figure S9). Likewise, the membrane hydrophobicity in this combined condition was demonstrated to be a reliable proxy for metabolic activity, in the form of cell growth and ethanol production in the combined inhibitory condition (Figure 7). The identification of lipid metric knobs to modulate membrane physical properties that impact metabolic activity can enable the prioritization of strains for characterization and also provide a possible selectable marker or proxy for metabolic activity. This can be useful when labs have limited resources and in the responsible execution of research funding.

The previous titration of *fabB* with inducible promoters showed the physiological relevance of unsaturated fatty acids in the cell membrane (Budin et al., 2018). The use of

inducible promoters in this prior study allowed for a carefully controlled set of experimental data, but the constitutive and varying strength promoters utilized in the work described here do not require the use of inducers, which could be attractive for larger-scale fermentations. Also, our goal was to demonstrate the general framework of probing these networks, not the design of strains for industrial applications or characterizing the function of specific enzymes.

This study was restricted to the membrane lipid composition and further analyses of other membrane elements that also might respond to stimuli and are important for membrane properties (e.g., phospholipid moieties, EPS content, outer membrane proteins, etc.) might enable additional layers for the prediction of metabolic activity.

The assessment of membrane hydrophobicity and membrane integrity are both relatively simple. Additionally, the hydrophobicity assay and flow cytometry provide the opportunity to sort cells based on their membrane properties, suggesting that a membrane property-based selection could be used in library enrichment or adaptive evolution, even allowing the selection of cells with low growth rate. These qualities of the physical membrane properties relevant to cell growth can offer insight to the challenges experienced by metabolic engineers in terms of the observed variability of biocatalysts robustness depending on the scale, mode of operation, and the specific composition of the cultures.

Among the three membrane physical properties used in our analysis, membrane hydrophobicity was strikingly impactful relative to membrane fluidity or integrity. This is consistent with previous studies (Chen et al., 2020) demonstrating the importance of this property, yet relatively few rational strategies for tuning hydrophobicity have been reported. Microbial hydrophobicity is also important in other areas such as biofilm formation and antimicrobial resistance where microbial adhesion to different surfaces and microbial proliferation is of interest.

5. ACKNOWLEDGEMENTS

characterization described here, and of Jennifer L. Reed.

6. REFERENCES

Alexander, R.A., 1990. A note on averaging correlations. Bull. Psychon. Soc. 28, 335–336.

Bligh, E.G., Dyer, W.J., 1959. A rapid method of total lipid extraction and purification. Can. J. Biochem. Physiol. 37, 911–917.

Bonamore, A., MacOne, A., Colotti, G., Matarese, R.M., Boffi, A., 2006. The desaturase from *Bacillus subtilis*, a promising tool for the selective olefination of phospholipids. J. Biotechnol. 121, 49-53.

Budin, I., Rond, T. de, Chen, Y., Chan, L.J.G., Petzold, C.J., Keasling, J.D., 2018. Viscous control of cellular respiration by membrane lipid composition. Science. 362, 1186–1189.

Caspeta, L., Chen, Y., Ghiaci, P., Feizi, A., Buskov, S., Hallström, B.M., Petranovic, D., Nielsen, J., 2014. Altered sterol composition renders yeast thermotolerant. Science. 346, 75–78.

Cerisy, T., Souterre, T., Torres-Romero, I., Boutard, M., Dubois, I., Patrouix, J., Labadie, K., Berrabah, W., Salanoubat, M., Doring, V., Tolonen, A.C., 2017. Evolution of a biomass-fermenting bacterium to resist lignin phenolics. Appl. Environ. Microbiol. 83, 1-13.

Curran, J.S., Smith, J., Holms, W., 1989. Heat-and-power in industrial fermentation processes. Appl. Energy 34, 9–20.

Chang, Y.Y., Cronan, J.E., 1999. Membrane cyclopropane fatty acid content is a major factor in acid resistance of *Escherichia coli*. Mol. Microbiol. 33, 249-259.

Chen, R.F., Bowman, R.L., 1965. Fluorescence polarization: Measurement with ultraviolet-polarizing filters in a spectrophotofluorometer. Science. 147, 729–732.

Chen, Y., Boggess, E.E., Ocasio, E.R., Warner, A., Kerns, L., Drapal, V., Gossling, C., Ross, W., Gourse, R.L., Shao, Z., Mansell, T.J., Jarboe, L.R., 2020. Reverse engineering of fatty acid-tolerant *Escherichia coli* identifies design strategies for robust microbial cell factories. Metab. Eng. 61, 120-130.

Chen, Y., Reinhardt, M., Neris, N., Kerns, L., Mansell, T.J., Jarboe, L.R., 2018. Lessons in Membrane Engineering for Octanoic Acid Production from Environmental *Escherichia coli* Isolates. Appl. Environ. Microbiol. 84, 1-14.

Chen, Y.Y., Gänzle, M.G., 2016. Influence of cyclopropane fatty acids on heat, high pressure, acid and oxidative resistance in *Escherichia coli*. Int. J. Food Microbiol. 222, 16–22.

Chi, Z., Zhao, X., Daugaard, T., Dalluge, D., Rover, M., Johnston, P., Salazar, A.M., Santoscoy, M.C., Smith, R., Brown, R.C., Wen, Z., Zabotina, O.A., Jarboe, L.R., 2019. Comparison of product distribution, content and fermentability of biomass in a hybrid thermochemical/biological processing platform. Biomass and Bioenergy 120, 107–116.

Cronan, J.E., Birge, C.H., Vagelos, P.R., 1969. Evidence for two genes specifically involved in unsaturated fatty acid biosynthesis in *Escherichia coli*. J. Bacteriol. 100, 601–604.

Cronan, J.E., Gelmann, E.P., 1973. An estimate of the minimum amount of unsaturated fatty acid required for growth of *Escherichia coli*. J. Biol. Chem. 248, 1188–1195.

Datsenko, K.A., Wanner, B.L., 2000. One-step inactivation of chromosomal genes in *Escherichia coli* K-12 using PCR products. Proc. Natl. Acad. Sci. 97, 6640–6645.

Ding, M.Z., Wang, X., Yang, Y., Yuan, Y.J., 2011. Metabolomic study of interactive effects of phenol, furfural, and acetic acid on *Saccharomyces cerevisiae*. Omi. A J. Integr. Biol. 15, 647-653.

Dombek, K.M., Ingram, L.O., 1984. Effects of ethanol on the *Escherichia coli* plasma membrane. J. Bacteriol. 157, 233-239.

Dunlop, M.J., Dossani, Z.Y., Szmidt, H.L., Chu, H.C., Lee, T.S., Keasling, J.D., Hadi, M.Z., Mukhopadhyay, A., 2011. Engineering microbial biofuel tolerance and export using efflux pumps. Mol. Syst. Biol. 7, 1–7.

Eaton, L.C., Tedder, T.F., Ingram, L.O., 1982. Effects of fatty acid composition on the sensitivity of membrane functions to ethanol in *Escherichia coli*. Subst. Alcohol Actions. Misuse. 3, 77–87.

Fletcher, E., Pilizota, T., Davies, P.R., McVey, A., French, C.E., 2016. Characterization of the effects of n-butanol on the cell envelope of *E. coli*. Appl. Microbiol. Biotechnol. 100, 9653–9659.

Foo, J.L., Jensen, H.M., Dahl, R.H., George, K., Keasling, J.D., Lee, T.S., Leong, S., Mukhopadhyay, A., 2014. Improving microbial biogasoline production in *Escherichia coli* using tolerance engineering. MBio. 5, 1-9.

Ghai, I., Ghai, S., 2018. Understanding antibiotic resistance via outer membrane permeability. Infect. Drug Resist. 11, 523–530.

Ghosh, I.N., Martien, J., Hebert, A.S., Zhang, Y., Coon, J.J., Amador-Noguez, D., Landick, R., 2019. OptSSeq explores enzyme expression and function landscapes to maximize isobutanol production rate. Metab. Eng. 52, 324–340.

Gong, Z., Nielsen, J., Zhou, Y.J., 2017. Engineering Robustness of Microbial Cell Factories. Biotechnol. J. 12, 1-9.

Grandvalet, C., Assad-García, J.S., Chu-Ky, S., Tollot, M., Guzzo, J., Gresti, J., Tourdot-Maréchal, R., 2008. Changes in membrane lipid composition in ethanol- and acid-adapted *Oenococcus oeni* cells: Characterization of the *cfa* gene by heterologous complementation. Microbiology. 154, 2611-2619.

Grogan, D W, Cronan, J.E., 1997. Cyclopropane ring formation in membrane lipids of bacteria. Microbiol. Mol. Biol. Rev. 61, 429–441.

Halverson, L.J., Firestone, M.K., 2000. Differential effects of permeating and nonpermeating solutes on the fatty acid composition of *Pseudomonas putida*. Appl. Environ. Microbiol. 66, 2414-2421.

Huffer, S., Clark, M.E., Ning, J.C., Blanch, H.W., Clark, D.S., 2011. Role of Alcohols in Growth, Lipid Composition, and Membrane Fluidity of Yeasts, Bacteria, and Archaea. Appl. Environ. Microbiol. 77, 6400–6408.

Ingram, L. O., 1976. Adaptation of Membrane Lipids to Alcohols'. J. Bacteriol. 125, 670–678.

Jarboe, L.R., 2018. Improving the success and impact of the metabolic engineering design, build, test, learn cycle by addressing proteins of unknown function. Curr. Opin. Biotechnol. 53, 93–98.

Jarboe, L.R., Klauda, J.B., Chen, Y., Davis, K.M., Santoscoy, M.C., 2018. Engineering the Microbial Cell Membrane To Improve Bioproduction, in: Cheng, H.N., Gross, R.A., Smith, P.B. (Eds.), Green Polymer Chemistry: New Products, Processes, and Applications, American Chemical Society. pp. 25–39. https://doi.org/10.1021/bk-2018-1310.ch003

Jezierska, S., Van Bogaert, I.N.A., 2017. Crossing boundaries: the importance of cellular membranes in industrial biotechnology. J. Ind. Microbiol. Biotechnol. 44, 721-733.

Jiang, X.R., Wang, H., Shen, R., Chen, G.Q., 2015. Engineering the bacterial shapes for enhanced inclusion bodies accumulation. Metab. Eng. 29, 227-237.

Kaplan, E., Greene, N.P., Crow, A., Koronakis, V., 2018. Insights into bacterial lipoprotein

trafficking from a structure of LolA bound to the LolC periplasmic domain. Proc. Natl. Acad. Sci. 115, 7389–97.

Khakbaz, P., Klauda, J.B., 2015. Probing the importance of lipid diversity in cell membranes via molecular simulation. Chem. Phys. Lipids. 192, 12-22.

Koga, Y., 2012. Thermal Adaptation of the Archaeal and Bacterial Lipid Membranes. Archaea 2012, 1–6.

Lennen, R M, Pfleger, B.F., 2013. Modulating Membrane Composition Alters Free Fatty Acid Tolerance in *Escherichia coli*. PLoS One 8, 54031. https://doi.org/10.1371/journal.pone.0054031

Liao, C., Liang, X., Yang, F., Soupir, M.L., Howe, A.C., Thompson, M.L., Jarboe, L.R., 2017. Allelic Variation in Outer Membrane Protein A and Its Influence on Attachment of *Escherichia coli* to Corn Stover. Front. Microbiol. 8, 708. https://doi.org/10.3389/fmicb.2017.00708

Liu, L., Pan, A., Spofford, C., Zhou, N., Alper, H.S., 2015. An evolutionary metabolic engineering approach for enhancing lipogenesis in *Yarrowia lipolytica*. Metab. Eng. 29, 36-45.

Liu, P., Chernyshov, A., Najdi, T., Fu, Y., Dickerson, J., Sandmeyer, S., Jarboe, L., 2013. Membrane stress caused by octanoic acid in *Saccharomyces cerevisiae*. Appl. Microbiol. Biotechnol. 97, 3239–3251.

Lu, J., Tang, J., Liu, Y., Zhu, X., Zhang, T., Zhang, X., 2012. Combinatorial modulation of *galP* and *glk* gene expression for improved alternative glucose utilization. Appl. Microbiol. Biotechnol. 93, 2455–2462.

Luo, L.H., Seo, P.-S., Seo, J.-W., Heo, S.-Y., Kim, D.-H., Kim, C.H., 2009. Improved ethanol tolerance in *Escherichia coli* by changing the cellular fatty acids composition through genetic manipulation. Biotechnol. Lett. 31, 1867–1871.

Mills, T.Y., Sandoval, N.R., Gill, R.T., 2009. Cellulosic hydrolysate toxicity and tolerance mechanisms in *Escherichia coli*. Biotechnol. Biofuels 2, 26. https://doi.org/10.1186/1754-6834-2-26

Minty, J.J., Lesnefsky, A.A., Lin, F., Chen, Y., Zaroff, T.A., Veloso, A.B., Xie, B., McConnell, C.A., Ward, R.J., Schwartz, D.R., Rouillard, J.M., Gao, Y., Gulari, E., Lin, X.N., 2011. Evolution combined with genomic study elucidates genetic bases of isobutanol tolerance in *Escherichia coli*. Microb. Cell Fact. 10, 18. https://doi.org/10.1186/1475-2859-10-18

Monje-Galvan, Viviana; Warburton, Linnea and Klauda, J.B., 2019. Setting Up All-Atom Molecular Dynamics Simulations to Study the Interactions of Peripheral Membrane Proteins with Model Lipid Bilayers, in: Intracellular Lipid Transport: Methods and Protocols, Methods in Molecular Biology. pp. 325–339. https://doi.org/10.7551/mitpress/1247.003.0036

Mukhopadhyay, A., 2015. Tolerance engineering in bacteria for the production of advanced biofuels and chemicals. Trends Microbiol. 23, 498–508.

Mykytczuk, N.C.S., Trevors, J.T., Leduc, L.G., Ferroni, G.D., 2007. Fluorescence polarization in studies of bacterial cytoplasmic membrane fluidity under environmental stress. Prog. Biophys. Mol. Biol. 95, 60–82.

Neidhardt, F.C., Bloch, P.L., Smith, D.F., 1974. Culture medium for enterobacteria. J. Bacteriol. 119, 736–747.

Okuyama, H., Saitoh, M., Hiramatsu, R., 1982. Fatty Acid Synthetase System in the Regulation of Membrane Lipid Synthesis in *Escherichia coli* after Shifts in Temperature*. J. Bio.

Chem. 257, 4812-4817.

Pembrey, R.S., Marshall, K.C., Schneider, R.P., 1999. Cell surface analysis techniques: What do cell preparation protocols do to cell surface properties? Appl. Environ. Microbiol. 65, 2877–94.

Poger, D., Caron, B., Mark, A.E., 2014. Effect of methyl-branched fatty acids on the structure of lipid bilayers. J. Phys. Chem. B. 118, 13838-13848.

Poger, D., Mark, A.E., 2015. A Ring to Rule Them All: The Effect of Cyclopropane Fatty Acids on the Fluidity of Lipid Bilayers. J. Phys. Chem. B. 119, 5487–5495.

Portnoy, V.A., Bezdan, D., Zengler, K., 2011. Adaptive laboratory evolution-harnessing the power of biology for metabolic engineering. Curr. Opin. Biotechnol. 22, 590-594.

Qi, Y., Liu, H., Chen, X., Liu, L., 2019. Engineering microbial membranes to increase stress tolerance of industrial strains. Metab. Eng. 53, 24-34.

Reyes, L.H., Almario, M.P., Kao, K.C., 2011. Genomic library screens for genes involved in n-butanol tolerance in *Escherichia coli*. PLoS One 6. https://doi.org/10.1371/journal.pone.0017678

Rolfe, M.D., Rice, C.J., Lucchini, S., Pin, C., Thompson, A., Cameron, A.D.S., Alston, M., Stringer, M.F., Betts, R.P., Baranyi, J., Peck, M.W., Hinton, J.C.D., 2012. Lag Phase Is a Distinct Growth Phase That Prepares Bacteria for Exponential Growth and Involves Transient Metal Accumulation. J. Bacteriol. 194, 686–701.

Rosenberg, M., Gutnick, D., Rosenberg, E., 1980. Adherence of bacteria to hydrocarbons: A simple method for measuring cell-surface hydrophobicity. FEMS Microbiol. Lett. 9, 29–33.

Royce, L.A., Liu, P., Stebbins, M.J., Hanson, B.C., Jarboe, L.R., 2013. The damaging effects of short chain fatty acids on *Escherichia coli* membranes. Appl. Microbiol. Biotechnol. 97, 8317–8327.

Rutherford, B.J., Dahl, R.H., Price, R.E., Szmidt, H.L., Benke, P.I., Mukhopadhyay, A., Keasling, J.D., 2010. Functional genomic study of exogenous n-butanol stress in *Escherichia coli*. Appl. Environ. Microbiol. 76, 1935-1945.

Ryan, K.R., Taylor3, J.A., Bowers Correspondence, L.M., 2010. The BAM complex subunit BamE (SmpA) is required for membrane integrity, stalk growth and normal levels of outer membrane b-barrel proteins in *Caulobacter crescentus*. Microbiology 156, 742–756.

Sandoval, N.R., Papoutsakis, E.T., 2016. Engineering membrane and cell-wall programs for tolerance to toxic chemicals: Beyond solo genes. Curr. Opin. Microbiol. 33, 56–66.

Santoscoy, M.C., Jarboe, L.R., 2019. Streamlined assessment of membrane permeability and its application to membrane engineering of *Escherichia coli* for octanoic acid tolerance. J. Ind. Microbiol. Biotechnol. 46, 843-853.

Scheel, M., Lütke-Eversloh, T., 2013. New options to engineer biofuel microbes: Development and application of a high-throughput screening system. Metab. Eng. 17, 51–58.

Šeputienė, V., Daugelavičius, A., Sužiedėlis, K., Sužiedėlienė, E., 2006. Acid response of exponentially growing *Escherichia coli* K-12. Microbiol. Res. 161, 65–74.

Shabala, L., Ross, T., 2008. Cyclopropane fatty acids improve *Escherichia coli* survival in acidified minimal media by reducing membrane permeability to H+ and enhanced ability to extrude H+. Res. Microbiol. 159, 458–461.

Sherkhanov, S., Korman, T.P., Bowie, J.U., 2014. Improving the tolerance of *Escherichia coli* to medium-chain fatty acid production. Metab. Eng. 25, 1-7.

Shinitzky, M., Barenholz, Y., 1978. Fluidity parameters of lipid regions determined by fluorescence polarization. BBA - Rev. Biomembr. 515, 367-394.

Shirley, S.G., Robinson, C.J., Dodd, G.H., 1987. The influence of temperature and membrane-fluidity changes on the olfactory adenylate cyclase of the rat. Biochem. J. 245, 613-616.

Steen, E.J., Kang, Y., Bokinsky, G., Hu, Z., Schirmer, A., McClure, A., Del Cardayre, S.B., Keasling, J.D., 2010. Microbial production of fatty-acid-derived fuels and chemicals from plant biomass. Nature. 463, 559-562.

Szekely, P., Dvir, T., Asor, R., Resh, R., Steiner, A., Szekely, O., Ginsburg, A., Mosenkis, J., Guralnick, V., Dan, Y., Wolf, T., Tamburu, C., Raviv, U., 2011. Effect of temperature on the structure of charged membranes. J. Phys. Chem. B. 115, 14501-14506.

Tan, Z., Black, W., Yoon, J.M., Shanks, J. V., Jarboe, L.R., 2017a. Improving *Escherichia coli* membrane integrity and fatty acid production by expression tuning of FadL and OmpF. Microb. Cell Fact. 16, 38. https://doi.org/10.1186/s12934-017-0650-8

Tan, Z., Khakbaz, P., Chen, Y., Lombardo, J., Yoon, J.M., Shanks, J. V., Klauda, J.B., Jarboe, L.R., 2017b. Engineering *Escherichia coli* Membrane Phospholipid Head Distribution Improves Tolerance and Production of Biorenewables. Metab. Eng. 44, 1-12.

Tan, Z., Yoon, J.M., Nielsen, D.R., Shanks, J. V., Jarboe, L.R., 2016. Membrane engineering via trans unsaturated fatty acids production improves *Escherichia coli* robustness and production of biorenewables. Metab. Eng. 35, 105–113.

Trček, J., Mira, N.P., Jarboe, L.R., 2015. Adaptation and tolerance of bacteria against acetic acid. Appl. Microbiol. Biotechnol. 99, 6215-6229.

Wang, A., Cronan, J.E., 1994. The growth phase-dependent synthesis of cyclopropane fatty acids in *Escherichia coli* is the result of an RpoS(KatF)-dependent promoter plus enzyme instability. Mol. Microbiol. 11, 1009–1017.

Wehrs, M., Tanjore, D., Eng, T., Lievense, J., Pray, T.R., Mukhopadhyay, A., 2019. Engineering Robust Production Microbes for Large-Scale Cultivation. Trends Microbiol. 27, 524-537.

Westbrook, A.W., Ren, X., Moo-Young, M., Chou, C.P., 2018. Engineering of cell membrane to enhance heterologous production of hyaluronic acid in *Bacillus subtilis*. Biotechnol. Bioeng. 115, 216-231.

Wikström, M., Kelly, A.A., Georgiev, A., Eriksson, H.M., Klement, M.R., Bogdanov, M., Dowhan, W., Wieslander, Å., 2009. Lipid-engineered *Escherichia coli* membranes reveal critical lipid headgroup size for protein function. J. Biol. Chem. 284, 954-965.

Wilbanks, B., Trinh, C.T., 2017. Comprehensive characterization of toxicity of fermentative metabolites on microbial growth. Biotechnol. Biofuels 10, 262. https://doi.org/10.1186/s13068-017-0952-4

Wu, T., Ye, L., Zhao, D., Li, S., Li, Q., Zhang, B., Bi, C., 2018. Engineering membrane morphology and manipulating synthesis for increased lycopene accumulation in *Escherichia coli* cell factories. 3 Biotech 8, 269. https://doi.org/10.1007/s13205-018-1298-8

Wu, W., Long, M.R., Zhang, X., Reed, J.L., Maravelias, C.T., 2018. A framework for the identification of promising bio-based chemicals. Biotechnol. Bioeng. 115, 2328–2340.

Xiao, X., Yu, X., Khosla, C., 2013. Metabolic Flux between Unsaturated and Saturated Fatty Acids Is Controlled by the FabA:FabB Ratio in the Fully Reconstituted Fatty Acid Biosynthetic Pathway of *Escherichia coli*. Biochemistry 52, 8304–8312.

Xie, F., Li, G., Zhang, W., Zhang, Y., Zhou, L., Liu, Shuanghong, Liu, Siguo, Wang, C., 2016. Outer membrane lipoprotein VacJ is required for the membrane integrity, serum resistance and biofilm formation of *Actinobacillus pleuropneumoniae*. Vet. Microbiol. 183, 1–8.

Young, E.M., Zhao, Z., Gielesen, B.E.M., Wu, L., Benjamin Gordon, D., Roubos, J.A., Voigt, C.A., 2018. Iterative algorithm-guided design of massive strain libraries, applied to itaconic

acid production in yeast. Metab. Eng. 48, 33–43.

Yuk, H.-G., Marshall, D.L., 2005. Influence of acetic, citric, and lactic acids on *Escherichia coli* O157:H7 membrane lipid composition, verotoxin secretion, and acid resistance in simulated gastric fluid. J. Food Prot. 68, 673–679.

Zaldivar, J., Ingram, L.O., 1999. Effect of organic acids on the growth and fermentation of ethanologenic *Escherichia coli* LY01. Biotechnol. Bioeng. 66, 203–210.

Zaldivar, J., Martinez, A., Ingram, L.O., 2000. Effect of alcohol compounds found in hemicellulose hydrolysate on the growth and fermentation of ethanologenic *Escherichia coli*. Biotechnol. Bioeng. 68, 524-530.

Zaldivar, J., Martinez, A., Ingram, L.O., 1999. Effect of selected aldehydes on the growth and fermentation of ethanologenic *Escherichia coli*. Biotechnol. Bioeng. 65, 24–33.

Zhang, X.-S., García-Contreras, R., Wood, T.K., 2007. YcfR (BhsA) influences *Escherichia coli* biofilm formation through stress response and surface hydrophobicity. J. Bacteriol. 189, 3051–3062.

Zhang, X., Jantama, K., Moore, J.C., Jarboe, L.R., Shanmugam, K.T., Ingram, L.O., 2009. Metabolic evolution of energy-conserving pathways for succinate production in *Escherichia coli*. Proc. Natl. Acad. Sci. 106, 20180-20185.

Zhang, Y.-M., Rock, C.O., 2008. Membrane lipid homeostasis in bacteria. Nat. Rev. Microbiol. 6, 222–233.

Zhao, X., Davis, K., Brown, R., Jarboe, L., Wen, Z., 2015. Alkaline treatment for detoxification of acetic acid-rich pyrolytic bio-oil for microalgae fermentation: Effects of alkaline species and the detoxification mechanisms. Biomass and Bioenergy. 80, 203-212.

7. FIGURE LEGENDS

Figure 1. Modulation of membrane lipid composition as a strategy for engineering robustness. The wild-type cell membrane (left panel) is often damaged during growth in inhibitory conditions (inhibitors). These growth inhibitory conditions also perturb gene expression (level 1), which results in modification of the membrane lipid composition, which can be quantified and described with metrics such as the relative abundance of unsaturated lipids (level 2), and with direct measurements of membrane physical properties (level 3). These changes and cell membrane responses occur in a fashion according to the chemistry of each compound and together they affect the overall health and metabolic activity of the organism, reflected in its growth and productivity (level 4). (Right) The expression tuning of previously reported genes for modulating the abundance of lipids with unsaturated acyl chains (*fabA*, *fabB* and *des*) is expected to produce a range of membrane compositions in the presence of various microbial inhibitors. This perturbation of membrane lipid parameters can be viewed as the turning of "knobs" in order to implement a change in "output" signals such as membrane properties, with the goal of improving growth and productivity.

Figure 2. Altered expression of *des*, *fabB* and *fabA* impacts membrane lipid composition in the baseline condition. Each gene was expressed under the control of three different promoters. From the weakest to the strongest, M1-12, M1-37 and M1-93 promoters were used for each of the three enzymes, resulting in nine engineered strains. For example, the M1-12-des construct is referred to as des12. (A) The relative abundance of unsaturated fatty acids increased compared to the control strain in five out of nine engineered strains. (B) Altered expression of *des*, *fabB* and *fabA* also impacted the average lipid length and (C) the relative abundance of cyclic fatty acids. (D) The ratio of linear chain fatty acids relative to the non-linear chain fatty acids in the cell membrane (L/nL ratio) also varied. Membrane physical properties are shown in Figure S4. All cells were grown in MOPS 2.0 w/v% dextrose at 37 ºC with shaking at 200 rpm and harvested during mid-log growth. All lipid metrics were calculated from the relative abundance of membrane fatty acids on a mass basis. All values are the average of three replicates with error bars indicating the standard deviation. Significant changes were determined relative to control strain (black) and are denoted as follows: *($p<0.05$), **($p<0.01$), ***($p<0.001$).

Figure 3. Some lipid composition metrics show significant associations during growth in the baseline condition. (A) Correlation matrix showing the relationship between knobs (level 2: membrane lipid distribution) and outcomes (level 3: membrane physical properties and level 4: cell growth) across the set of ten strains in the baseline condition. The numerical values are the correlation coefficients (R^2), with red shading indicating positive correlation and blue shading indicating negative correlation. Those shown in bold rectangles were found to be not random ($p<0.05$). (B) Significant correlation of the L/nL ratio and the average lipid length. All data points and values represent the average of three biological replicates and the percentage of the coefficient of variation was less than 10% for all samples. All strains were grown in MOPS 2% w/v dextrose at 37 °C.

Figure 4. Perturbation of membrane lipid distribution impacts specific growth rate during challenge with industrially relevant cell growth inhibitors. The majority of the nine engineered strains showed increased tolerance for (A) high temperature (42 °C) and (B) furfural. However, only a few strains showed tolerance towards (C) acetate, (D) acidified media (pH 6.00), (E) ethanol, or (F) butanol. None of the strains showed tolerance or sensitivity to the other two tested conditions ((G) isobutanol and (H) hexanol). Concentrations of alcohols are expressed as a percentage of the volume of alcohol relative to volume of culture media. All values are the average of three replicates with error bars indicating the standard deviation. Significant changes relative to control strain (black) are denoted as follows: *($p<0.05$), **($p<0.01$), ***($p<0.001$).

Figure 5. Perturbed expression of *des*, *fabA* and *fabB* has an inhibitor-dependent impact on the membrane lipid composition and membrane properties. Membrane lipid metrics (knobs, top panel) and membrane properties (outcomes, bottom panel) were determined for each strain and the range of values is shown as a whisker plot. The control strain is shown as a red bar. Knobs: (A) the levels of unsaturation, (B) lipid lengths, (C) abundance of cyclic rings in the cell membrane, and (D) ratio of linear and non-linear acyl chains. Outcomes: (E) hydrophobicity, (F) membrane DPH polarization, (G) permeability. Depending on the culture condition, different ranges for each membrane metric were observed. Symbol (+) in furfural condition indicates that strains fabB93 and fabA93 are not shown in this plot for this condition. The data for these strains

can be found in Figure S6. Whisker plots were constructed with the average of three biological replicates for each strain in each condition, with a percentage coefficient of variation of less than 10% for all samples. Whiskers indicate the strain with the minimum and the maximum value for each condition, and the shaded box depicts the values between the lower (Q2) and the upper (Q3) quartiles of the ranges. Only strains with values outside Q2 and Q3 quartiles are color coded, using the color scheme established in Figure 2, with blue for *des* strains, orange for *fabB* strains, green for *fabA* strains and the intensity of the color increasing with promoter strength from 12 to 37 to 93.

Figure 6. Systematic characterization of knobs and outcomes enabled generation of overall and individual-condition response networks and correlations.

The modulated knobs (% U: percentage of unsaturated fatty acids, LL: lipid length, %C: percentage of cyclic rings, and L/nL: ratio of linear and non-linear fatty acids) and outcomes (PL: polarization, HP: hydrophobicity, PM: permeability, and growth) showed different correlations for the overall and inhibitor-specific conditions. The numerical values are correlation coefficients (R^2), with significant correlations shown in a bold black square. Lines are shown in color only for significant connections, based on non-random linear regression. Red lines indicate positive correlation and blue lines indicate negative correlation.

(I) A general response network was generated using the data from all of the tested individual inhibitory conditions.

(II) Each inhibitor also had specific responses and correlations between knobs and outcomes. The convention for letter coding for each inhibitor was previously introduced in Figure 4. The thickness of the lines represents the number of conditions in which the significant correlation was observed.

(III) The correlation coefficients varied across individual inhibitors, with some conditions producing stronger or weaker connections between knobs and outcomes.

Figure 7. Membrane hydrophobicity is a significant predictor of strain performance

Membrane hydrophobicity and specific growth rates of the strains were assessed in the combined condition of 2.5 mM furfural and 2% v/v ethanol at 42 °C. Ethanol production was determined when the set of strains harboring the pKS13 plasmid were cultured for 24 h in the baseline condition with 5 mM furfural at 42 °C.

(A) The experimental membrane hydrophobicity in the triple condition significantly ($p<0.05$) correlated with growth rates in the triple condition. (B) The experimental membrane hydrophobicity in the triple inhibitory condition significantly correlated to ethanol productivity in combined condition with 5mM furfural at 42 °C. (C) Specific growth rates in the triple condition did not correspond to ethanol productivity.

All data points represent the average of three biological replicates, and the error bars indicate the standard deviations. Strains are color coded as in Figure 2.

Table 1. Strains and plasmids utilized in this study. The numerical designations correspond to

the promoters used to express the target gene.

Strains	Genotype	Reference
MG1655 (WT)	F- lambda- *ilvG*- *rfb*-50 *rph*-A	Jarboe's Lab
Control	MG1655, Δ*ldhA*::FRT-*cat*-FRT, Cm$^+$	(Tan et al., 2016)
FabA: β-hydroxyacyl-ACP dehydratase/isomerase		
fabA12	MG1655, Δ*ldhA*::M1-12-fabA-FRT-cat-FRT-bc1, Cm$^+$	This study
fabA37	MG1655, Δ*ldhA*::M1-37-fabA-FRT-cat-FRT-bc2, Cm$^+$	This study
fabA93	MG1655, Δ*ldhA*::M1-93-fabA-FRT-cat-FRT-bc3, Cm$^+$	This study
FabB: β-ketoacyl-ACP synthase I		
fabB12	MG1655, Δ*ldhA*::M1-12-fabB-FRT-cat-FRT-bc4, Cm$^+$	This study
fabB37	MG1655, Δ*ldhA*::M1-37-fabB-FRT-cat-FRT-bc5, Cm$^+$	This study
fabB93	MG1655, Δ*ldhA*::M1-93-fabB-FRT-cat-FRT-bc6, Cm$^+$	This study
Des: *B. subtilis* fatty acid desaturase		
des12	MG1655, Δ*ldhA*::M1-12-des-FRT-cat-FRT-bc7,Cm$^+$	This study
des37	MG1655, Δ*ldhA*::M1-37-des-FRT-cat-FRT-bc8, Cm$^+$	This study
des93	MG1655, Δ*ldhA*::M1-93-des-FRT-cat-FRT-bc9, Cm$^+$	This study
Plasmid pKS13	PBBR vector backbone, pdc, adhB, Tet$^+$	(Steen et al., 2010)
	PDC: *Zymomonas mobilis* pyruvate decarboxylase (*pdc*)	
	ADH2: *Z. mobilis* alcohol dehydrogenase (*adhB*)	

Table 2. Theoretical combined correlation coefficients of membrane metrics and cell growth rate in selected hypothetical multi-stressor scenarios. Results are shown only for scenarios in which there is continuity between membrane metrics predicted to impact cell growth and the confidence interval (standard deviation) of the calculated correlation coefficient is fully negative or fully positive. Full results of the 62 scenarios are given in Table S3. Color coding indicates the sign and the magnitude of the calculated combined correlation coefficients. Scenarios are presented in order of the two combined correlation coefficients. Each individual inhibitor is represented by a letter as in Figure 6: (A) 42 °C, (B) furfural, (C) acetate, (D) pH 6, (E) ethanol, (F) butanol, (G) isobutanol, and (H) hexanol. ***Experimentally validated scenario**.

Scenario	Lipid metric (knob)	Membrane property (output)	Combined correlation coefficient (L3)	Membrane metric to modulate growth	Combined correlation coefficient (L4)
furfural, acetate (B, C)	LL	PM	0.53 ± 0.06	LL	0.50 ± 0.06
*42 °C, furfural, ethanol (A, B, E)	**L/nL**	HP	**0.61 ± 0.03**	**HP**	**0.26 ± 0.05**
furfural, acetate, hexanol (B, C, H)	LL		-0.49 ± 0.26	LL	0.35 ± 0.21
42 °C, furfural (A, B)	L/nL		0.61 ± 0.05		0.22 ± 0.00
42 °C, butanol (A, F)	%U		-0.34 ± 0.25	HP	0.41 ± 0.23
42 °C, furfural, butanol (A, B, F)	L/nL		0.37 ± 0.34		0.34 ± 0.19
42 °C, acetate, isobutanol (A, C, G)	LL		-0.44 ± 0.24		0.26 ± 0.24

		Summary of knobs and outcomes that likely modulate growth			
		Knobs	# of scenarios	Outcomes	# of scenarios
		%U	1	PL	0
		LL	3	HP	5
		%C	0	PM	0
		L/nL	3		

8. SUPPLEMENTAL INFORMATION, FIGURES, TABLES AND METHODS

Supplemental Information

Experimental validation of selected lipid metrics to predict membrane hydrophobicity in multi-stressor conditions

In preparation for our experimental validation of the two selected combined conditions, we averaged the value of the relevant knob of each of the ten strains measured in each of the relevant individual inhibitory conditions. For example, for the 42ºC/furfural/ethanol condition, we averaged the individual L/nL values observed in the 42 ºC condition, the furfural condition and the ethanol condition. The average value for each strain was then normalized relative to the highest value within the strain set. Thus, each strain had a normalized average L/nL ratio for the triple condition and a normalized average lipid length for the acetate/hexanol condition, where these values were derived from the single-inhibitor experiments.

We then experimentally measured the membrane hydrophobicity for each of the ten strains in both of the scenarios with multiple stressors. This experimental data was normalized based on the highest observed value within the set of strains in that condition. It should be noted that the concentrations of furfural and ethanol were decreased by half with the goal of obtaining sufficient cell densities for experimental characterization. Thus, for the 42ºC/furfural/ethanol condition, each strain has an average normalized L/nL ratio and a normalized hydrophobicity that was directly determined by experimental characterization in the combined condition. For the acetate/hexanol condition, each strain similarly has an average normalized lipid length and normalized experimentally determined hydrophobicity.

We then evaluated the success of this approach. For the triple condition, if the L/nL ratios from the individual conditions still corresponded to the membrane hydrophobicity, then the range and distribution of the calculated average normalized L/nL ratios should correspond to the experimentally measured normalized hydrophobicity values. The difference between the normalized L/nL and the hydrophobicity for each strain can be calculated. For example, a normalized L/nL ratio of 1.00 and a normalized hydrophobicity of 0.1 would have an absolute difference of 0.9. Strains in the triple scenario had absolute differences that varied from 0.016 to 0.50, with an average value of 0.21 and sum of squared errors (SSE) of 0.74 when the normalized average L/nL ratio was utilized as predictor of the experimental normalized membrane hydrophobicity.

In the absence of the systematic approach used here, one might expect that the hydrophobicities in the individual condition could be used to predict the hydrophobicity in the triple condition. Thus, we performed similar calculations as described above, but replaced the L/nL ratio in the individual conditions with the hydrophobicity value. With this non-systematic approach, the average absolute difference was 0.30 and the SSE was 1.39, both of which are greater than the values observed using the L/nL ratio as the predictor (Figure S9 AB). This shows that the L/nL ratios from the single inhibitor experiments were better predictors of the hydrophobicity in the combined condition than the strain-specific hydrophobicities in the individual condition, emphasizing the utility of identifying the L/nL ratio-hydrophobicity connection.

The acetate/hexanol scenario had differences that varied from 0.00 to 0.99, with an average of 0.35 and SSE of 1.89 when the lipid length was utilized as the predictor of the hydrophobicity (Figure S9 C). The use of the hydrophobicities from the individual conditions to predict the hydrophobicities in presence of both acetate and hexanol gave an average absolute difference of 0.47 and SSE of 3.08. Thus, in both of these scenarios, the use of the lipid metric knob to predict the hydrophobicity in the multi-stressor condition was better than the use of the hydrophobicity in the single inhibitor condition, as evidenced by both the average absolute difference and the SSE.

To further validate the significance of these predictions, we performed a simulation in which the normalized hydrophobicity values were predicted 100 times based on randomly generated values between 0 and 1, with these random values serving as sham normalized metrics. For this simulation, the average absolute difference was 0.33, consistent with the known mean absolute difference of a continuous uniform distribution. Our use of the individual L/nL values to predict the membrane hydrophobicity in the triple scenario had a significantly lower average absolute difference than this random population ($p = 0.031$). This indicates that the L/nL ratios from the individual conditions, identified as the candidate knob based on the combined correlation coefficient, do correspond to the membrane hydrophobicity in the combined condition. For the acetate/hexanol condition, the use of the lipid length as the predictor was not significantly better than the random predictions ($p = 0.4$).

These results highlight the relevance of using a systematic approach to identify lipid metrics from individual-inhibitor conditions that can alter specific membrane properties when

cells are cultured in combined inhibitory conditions. This identification of a knob-outcome connection can be utilized in strain design. In addition, the identification of the most promising lipid metric knob can also guide the prioritization of strains for characterization in a multi-inhibitor condition, possibly increasing the efficiency of the build-test-learn component of the design-build-test-learn cycle.

Supplemental Figures and Tables
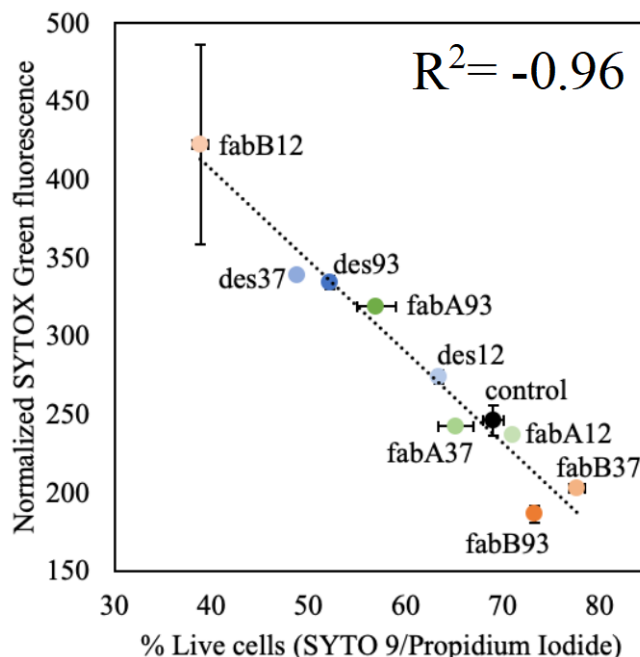
Figure S1. Viability assay correlated with membrane permeability assessment. These strains containing the pKS13 plasmid were cultured in 5 mM furfural at 42 °C in MOPS 2% w/v dextrose pH 7.00. Higher percentages of live cells correspond to lower membrane permeability values. Strains were harvested at 24 h for both assays.
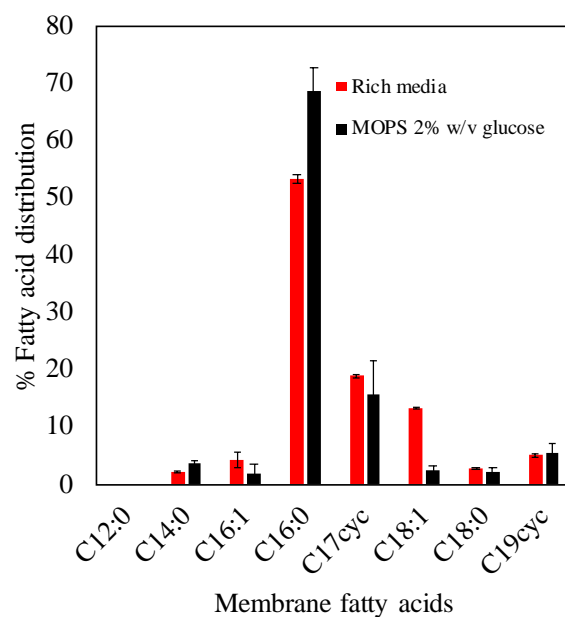
Figure S2. Membrane lipid composition of the control strain differs during growth in minimal and rich media. The control strain had higher abundance of unsaturated fatty acids, especially C18:1, when cultured in rich media relative to the baseline condition.
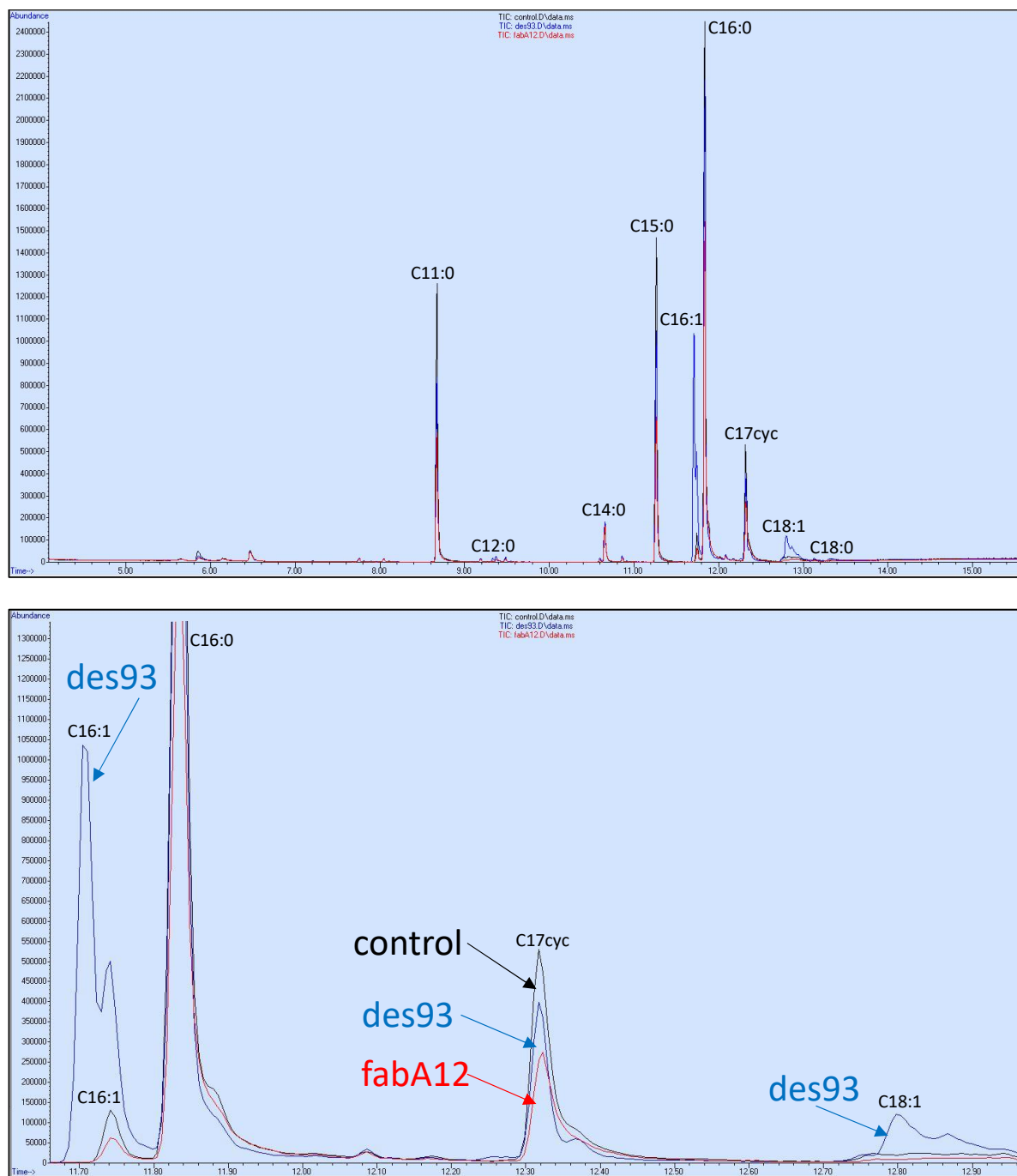
Figure S3. Total ion chromatograms of control, des93 and fabA12 strains. Engineered strain des93 (blue) showed a higher percentage of unsaturated fatty acids C16:1 and C18:1 relative to control (black) and fabA12 (red) strains when cultured in the baseline condition.
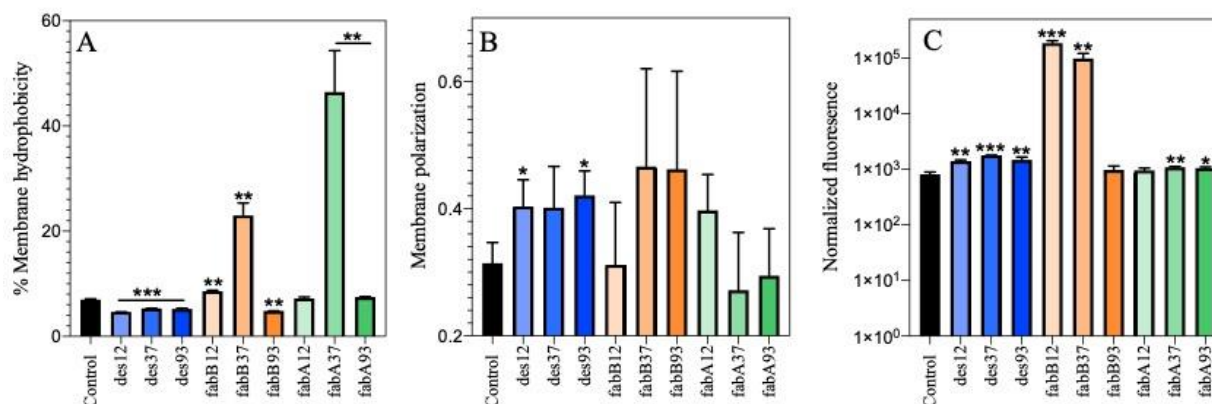
Figure S4. Membrane properties in the baseline condition. A) Membrane hydrophobicity was changed for the majority of strains. B) Membrane fluidity significantly decreased in the strains des93 and des12 despite their higher percentage of unsaturated fatty acids. C) Most strains showed altered membrane permeability. Strains fabB12 and fabB37 had orders of magnitude higher membrane permeability compared to control strain. Significant changes were relative to the control strain are denoted as follows: *($p < 0.05$), **($p < 0.01$), ***($p < 0.001$).

Figure S5. Percentage of change of the characterized membrane metrics for each type of engineered cell membrane during exposure to individual inhibitors relative to the baseline condition.
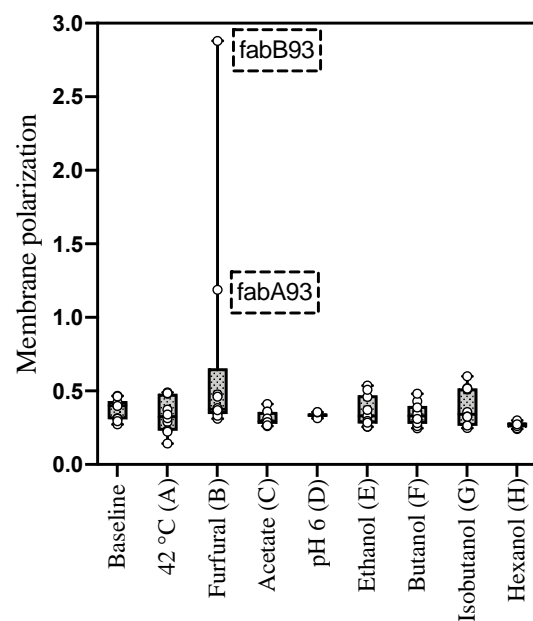
Figure S6. Membrane polarization in all inhibitory conditions. fabB93 and fabA93 showed a drastic decrease in membrane fluidity when cultured with 5 mM furfural. These two strains are not shown in the main text in order to better appreciate the changes in membrane fluidity caused by the other inhibitors. The correlation analyses considered all strains.
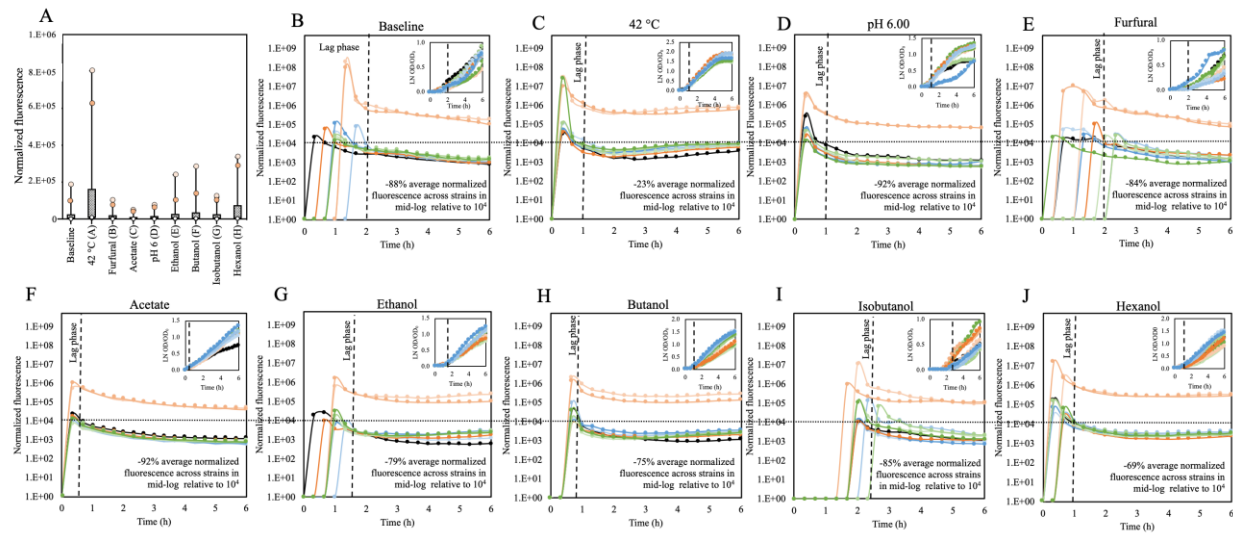
Figure S7. Membrane leakage shown by the perturbed membrane lipid composition set of strains when cultured in individual inhibitory conditions. Consistently, the strains faB12 and fabB37 had high membrane permeability values compared to the rest of strains. The correlation analysis considered only the mid-log data of all strains. The strains showed high membrane permeability during the lag phase across conditions. All strains had a normalized fluorescence higher than 10^4 in the lag phase. The 42 °C condition had the smallest decrease in membrane permeability during log phase relative to the lag-phase.
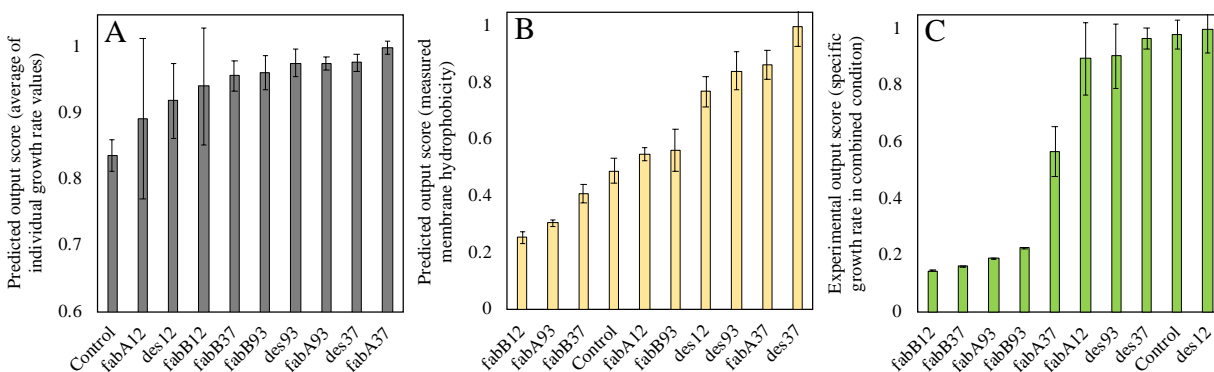
Figure S8. Output scores values for growth in combined condition with 2% v/v ethanol, 2.5 mM furfural in minimal media at 42 °C. This is the same data that is presented in the main text, but it is presented in a different format here.

(A) Specific growth rate values for each strain in each of the three individual conditions were averaged and normalized relative to the highest average value. (B) The membrane hydrophobicity value was measured for each strain in the combined culture condition and normalized. (C) The actual experimental growth rates of the set of *E. coli* strains cultured in the combined condition were normalized to the highest value producing the output scores. Note that the slowest-growing strain fabB12 also had the lowest membrane hydrophobicity and that, except for the control strain, the cluster of strains engineered with the Des enzyme produced the highest experimental output score for both membrane hydrophobicity B) and growth rate C).
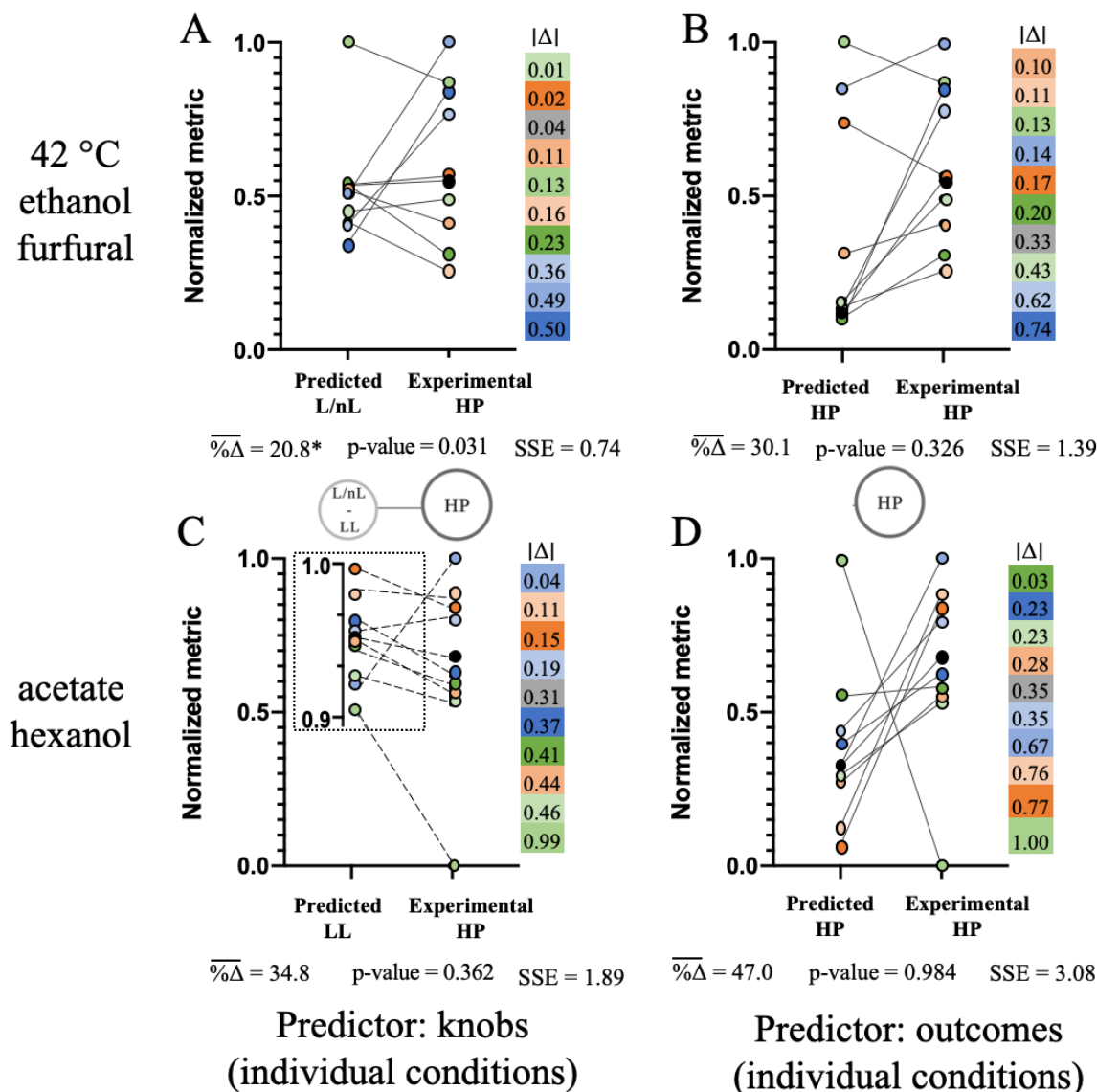
Figure S9. Membrane lipid metrics from individual conditions can be used to estimate the experimental membrane properties in multi-stressor conditions.

Membrane metrics from individual inhibitory conditions were utilized as predictors of experimental membrane hydrophobicity in combined inhibitory conditions based on the calculated combined correlation coefficients presented in Table 2.

(A) The normalized average L/nL ratios from the individual conditions of minimal media at 42 ºC, ethanol and furfural were utilized to estimate the normalized hydrophobicity measured for each strain (color coded dot) in the combined condition, with an average absolute difference ($\overline{\%\Delta}$) across the ten strains significantly lower (p = 0.03) than a random population.

(B) The use of the normalized average membrane hydrophobicities from the individual condition to estimate the normalized measured membrane hydrophobicity in the triple condition did not perform significantly better than a random population, with a $(\overline{\%\Delta})$ of 30.1. The sum of squared errors (SSE) also suggested that the L/nL ratio from individual conditions was more suitable than the membrane hydrophobicity from individual conditions to estimate the experimental membrane hydrophobicity in the combined triple condition.

(C) For the scenario with acetate and hexanol, the use of the normalized average lipid length from the individual conditions to predict the normalized hydrophobicity in the combined conditions was not significantly better than the random population $(\overline{\%\Delta} = 34.8)$. But, had a lower error (SSE=1.89) relative to (D) the use of the average normalized hydrophobicity from the individual conditions to predict the experimental membrane hydrophobicity in the combined condition (SSE= 3.08).

Each dot represents one strain, and the color code is the same as utilized in the main text.
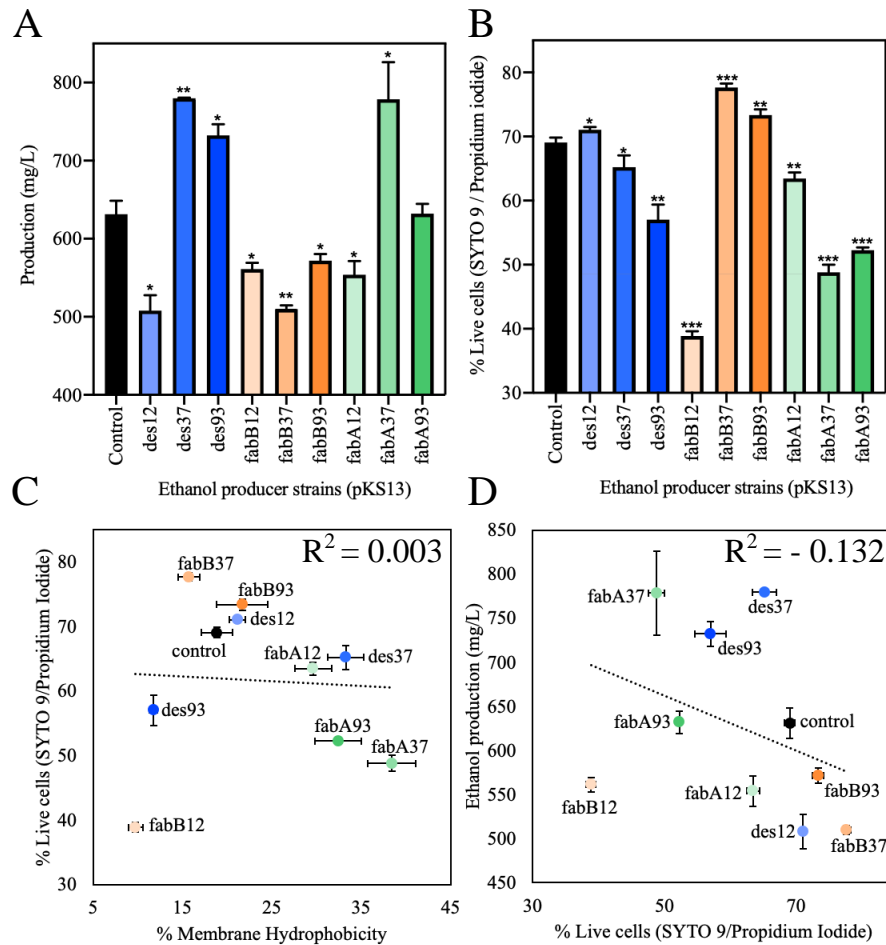
Figure S10. Cell viability did not correlate with membrane hydrophobicity or ethanol production. (A) Set of engineered strains with altered membrane lipid composition harboring the pKS13 plasmid showed significant differences in ethanol production. (B) Set of ethanol producer strains showed different percentage of cell viability. (C) Cell viability of the producer strains did not correspond neither to the experimental membrane hydrophobicity in the combined condition nor to (D) ethanol production in presence of 5 mM furfural at 42 °C in minimal media MOPS 2% w/v dextrose pH 7.00. Significant changes were determined relative to control strain (black) and are denoted as follows: *($p<0.05$), **($p<0.001$), ***($p<0.0001$).

Table S1. List of primers utilized for constructing set of *E. coli* strains utilized in this study.

#	Sequence (5'-3')	Note
1	AAAAAATTAGCGCAAGAAGACAAAAATCACCTTGCGCTAATGCTCTGTTACAGTCAGGCATTCTTCCGCAGCTTC	M1-12 promoter
2	AAATATTTTTAGTAGCTTAAATGTGATTCAACATCACTGGAGAAAGTCTTTTATCTCTGGCGGTGTTGAC	M1-37 promoter
3	AAATATTTTTAGTAGCTTAAATGTGATTCAACATCACTGGAGAAAGTCTTTTATCTCTGGCGGTGTTGAC	M1-93 promoter
4	GATTGCAGCATTACACGTCTTGAGC	*cat* gene from pKD3 plasmid
5	TTGTGCATTCGAAACTTACTCTATGTGCGACTTACAGAGGTATTGACACTTAACGGCTGACATGG	
6	AACGTCGGATGCGACGCTGGCGCGTCTACTCCGACCTACTGCGAATAGATTGCAGCATTACACGTC	
7	GGACCATGGCTAATTCCCATGGATCCGAGGTTTCGCCTTTTGATAC	
8	AAATATTTTTAGTAGCTTAAATGTGATTCAACATCACTGGAGAAAGTCTTTTATCTCTGGCGGTGTTGAC	
9	TCTGATTATAATCAGACAGAGTATCAAAAGGCGAAACCTCCACTTAACGGCTGACATGGG	
10	TATAATCAGACAGAGTATCAAAAGGCGAAACCTCGGATCCATGGGAATTAGCCATGGTCC	
11	ACCCCTAATAGACTTAGTCGAGGGGACCTTACGTCCCCTCGCCGTTCTAgtgtaggctggagctgcttc	
12	TTAGCGCAAGGTGATTTTTGTCTTCTTGCGCTAATTTTTTCACTTAACGGCTGACATGGG	fabA12
13	AGTCAGGAATTCTCATCGAATTTACACTAAGTTGTAGTGACCTCTTTCAGAATTTATCTCTGGCGGTGTTGAC	
14	CCCTTTTGGTGCGTCAGTCAGTTTAAACCAGGAAACAGCTATGGTAGATAAACGCGAATC	
15	AGGTCTTCTTTTGTATAGGATTCGCGTTTATCTACCATAGCTGTTTCCTGGTTTAAACTG	
16	CATATGGACCATGGCTAATTCCCATGTCAGCCGTTAAGTGGAGGTTTCGCCTTTTGATAC	
17	AGAGACCTCGTGTGCTACACAATTACCATAAGATTGCAGCATTACACGTC	
18	TATTCCGAAGTTCCTATTCTCTAGAAAGTATAGGAACTTCGAAGCAGCTCCAGCCTACAC	
19	TAAGAATAGAGGATGAAAGGTCATTGGGGATTATCTGAATCAGCTCCCC	
20	AGTCAGGAATTCTCATCG	
21	ACCCCTAATAGACTTAGTCG	
22	TCTCTCTGGAAGGTCTGACC	
23	GGGGATTATCTGAATCAGCTCC	
24	ATGAAACGTGCAGTGATTAC	*fabB* gene
25	AATTTAATCTTTCAGCTTGCGC	
26	CCAGAGGCAAGAAGGTCTTCTTTTGTATAGGATTCGCGTTTATCTACCATAGCTGTTTCCTGGTTTAAAC	fabA37
27	CACTGGCTCGTAATTTATTGTTTAAACCAGGAAACAGCTATGGTAGATAAACGCGAATCC	
28	TACGACTCACTATAGGGAGAGTGCAACATTGATAGATGGCAGAGACCTCGTGTGCTACAC	
29	GTGTAGCACACGAGGTCTCTGCCATCTATCAATGTTGCACTCTCCCTATAGTGAGTCGTA	
30	CCAGAGGCAAGAAGGTCTTCTTTTGTATAGGATTCGCGTTTATCTACCATAGCTGTTTCCTGGTTTAAAC	fabA93
31	CCGTATTGTTAGCATGTACGTTTAAACCAGGAAACAGCTATGGTAGATAAACGCGAATCC	
32	TACGACTCACTATAGGGAGAAGCGCCGCGTGAGACAATATAGAGACCTCGTGTGCTACAC	
33	GTGTAGCACACGAGGTCTCTATATTGTCTCACGCGGCGCTTCTCCCTATAGTGAGTCGTA	
34	GCTTTGTCAGCTGTTTTTGTTTATGTGCAATGGTTTGTTCAGTCATAGCTGTTTCCTGGTTTAAACTGAC	des12
35	CCCTTTTGGTGCGTCAGTCAGTTTAAACCAGGAAACAGCTATGACTGAACAAACCATTGCACATAAAC	
36	TACGACTCACTATAGGGAGAAGCGGTACTGAGGTATCATTAGAGACCTCGTGTGCTACAC	
37	CGAGGTCTCTAATGATACCTCAGTACCGCTTCTCCCTATAGTGAGTCGTA	
38	ACTTGCTTTGTCAGCTGTTTTTGTTTATGTGCAATGGTTTGTTCAGTCATAGCTGTTTCCTGGTTTAAAC	des37

39	CCACTGGCTCGTAATTTATTGTTTAAACCAGGAAACAGCTATGACTGAACAAACCATTGC	
40	CTACGACTCACTATAGGGAGACTTCACAGGCTGGTGTACGTAGAGACCTCGTGTGCTACA	
41	TGTAGCACACGAGGTCTCTACGTACACCAGCCTGTGAAGTCTCCCTATAGTGAGTCGTAG	
42	CTTGCTTTGTCAGCTGTTTTTGTTTATGTGCAATGGTTTGTTCAGTCATAGCTGTTTCCTGGTTTAAACG	des93
43	CCCGTATTGTTAGCATGTACGTTTAAACCAGGAAACAGCTATGACTGAACAAACCATTGC	
44	CTACGACTCACTATAGGGAGATGTGAGCTTGTTACTACGGCAGAGACCTCGTGTGCTACA	
45	TGTAGCACACGAGGTCTCTGCCGTAGTAACAAGCTCACATCTCCCTATAGTGAGTCGTAG	
46	TTACCGATGCTGGAAACAATGCCCAGGCCAGTAATCACTGCACGTTTCATAGCTGTTTCCTGGTTTAAAC	fabB12
47	CCCTTTTGGTGCGTCAGTCAGTTTAAACCAGGAAACAGCTATGAAACGTGCAGTGATTACTGGCCTG	
48	CATATGGACCATGGCTAATTCCCATGTCAGCCGTTAAGTGTGCGACGCTGGCGCGTCTAC	
49	TTAATTCGCAGTAGGTCGGAGTAGACGCGCCAGCGTCGCACACTTAACGGCTGACATGGG	
50	TACGACTCACTATAGGGAGACCTATACCTTACAACTGAGGAGAGACCTCGTGTGCTACAC	
51	GTGTAGCACACGAGGTCTCTCCTCAGTTGTAAGGTATAGGTCTCCCTATAGTGAGTCGTA	
52	TTACCGATGCTGGAAACAATGCCCAGGCCAGTAATCACTGCACGTTTCATAGCTGTTTCCTGGTTTAAAC	fabB37
53	AGCCACTGGCTCGTAATTTATTGTTTAAACCAGGAAACAGCTATGAAACGTGCAGTGATTACTGG	
54	TACGACTCACTATAGGGAGAAGTTCCGTGAGCGGCAATCAAGAGACCTCGTGTGCTACAC	
55	GTGTAGCACACGAGGTCTCTTGATTGCCGCTCACGGAACTTCTCCCTATAGTGAGTCGTA	
56	TTACCGATGCTGGAAACAATGCCCAGGCCAGTAATCACTGCACGTTTCATAGCTGTTTCCTGGTTTAAAC	fabB93
57	AGCCCGTATTGTTAGCATGTACGTTTAAACCAGGAAACAGCTATGAAACGTGCAGTGATTACTGG	
58	TACGACTCACTATAGGGAGAGTCCTATCTTCGGGTCTGGAAGAGACCTCGTGTGCTACAC	
59	GTGTAGCACACGAGGTCTCTTCCAGACCCGAAGATAGGACTCTCCCTATAGTGAGTCGTA	
60	CAATATCGCCATAGCTTTCAATTAAATTTGAAATTTTGTAAAATATTTTTAGTAGCTTAAATGT	confirm *ldhA* replacement
61	ATTGTGGTTCTCAATTACAGTTTCTGACTCAGGACTATTTTAAGAATAGAGGATGAAAGG	
62	CAACATCACTGGAGAAAGTC	
63	TAAGAATAGAGGATGAAAGGTC	
64	CAGCCTACGACTCACTATAG	

Table S2. Fold change of each membrane metric for the control strain relative to the baseline condition. This is the same data indicated by the red bars in Figure 5 but presented in a different form. The exposure of the control strain to (A) 42 °C, (B) Furfural, (C) Acetate, (D) pH 6, (E) Ethanol, (F) Butanol, (G) Isobutanol, or (H) Hexanol caused different fold-changes relative to the baseline condition for each membrane metric. Depending on the inhibitory condition, different membrane metrics in the control strain were altered. The percentage of unsaturated fatty acids was changed from 0 to 6-fold when the control strain was culture with either acetate or hexanol, respectively. Overall, the other membrane metrics did not have changes greater than 3-fold and in most cases, the inhibitors cause small change on the metrics relative to baseline condition.

	A	B	C	D	E	F	G	H
% Unsaturated FA	3.86	4.53	0.04	-0.58	2.58	4.86	2.91	6.08
Lipid length	0.03	0.02	0.02	0.00	0.00	0.02	0.02	0.02
Cyclic rings	0.00	-0.70	0.75	0.26	-0.43	-0.40	-0.12	-0.66
L/nL ratio	-0.58	-0.34	-0.50	-0.11	-0.19	-0.52	-0.44	-0.54
Hydrophobicity	1.95	0.00	-0.61	1.56	-1.04	-2.32	-1.00	0.64
Polarization	-0.08	0.18	-0.17	0.10	0.04	0.15	0.91	-0.09
Permeability	3.82	-0.75	0.43	0.52	-0.24	0.40	0.41	2.27

Table S3. Selected combined correlation coefficients for modulating membrane properties and growth in hypothetical combined scenarios. Each individual condition was assigned to a letter as follows: (A) 42 °C, (B) furfural, (C) acetate, (D) pH 6, (E) ethanol, (F) butanol, (G) isobutanol, and (H) hexanol. Each membrane lipid metric (LL: Lipid Length, %U: percentage of unsaturated fatty acids, %C: percentage of cyclic rings, and L/nL: ratio of linear relative to non-linear fatty acids) correlated with a membrane property (HP: Hydrophobicity, PL: Fluidity, and PM: Permeability) depending on the scenario (Level 3 modulation, L3). Likewise, measurement of membrane properties can be suitable to predict growth from several potential combined scenarios (Level 4 modulation, L4). Experimentally validated scenarios to predict membrane properties (L3*), and growth (L3, L4**) are shown in red boxes. Several scenarios showed similar or higher combined correlation coefficients than the experimentally validated combined conditions.

Number	Scenario	Lipid metric (knob)	Membrane property (output)	Likelihood index (L3)	Membrane property to modulate growth	Likelihood index (L4)
1	A,B	L/nL	PL	0.61	HP	0.23
2	A,C	LL	HP	0.62	HP	0.29
3	A,D	L/nL	HP	0.43	HP	0.13
4	A,E	L/nL	HP	0.63	HP	0.28
5	A,F	%U	HP	0.35	PL	0.43
6	A,G	L/nL	PL	0.51	HP	0.28
7	A,H	%U	PL	0.66	HP	0.12
8	B,C	LL	PM	0.54	HP	0.38
9	B,D	LL	PM	0.43	PL or HP	0.13
10	B,E	L/nL	HP	0.59	HP	0.27
11	B,F	LL	PM	0.39	PL	0.42
12	B,G	LL	PM	0.31	HP	0.39
13	B,H	L/nL	HP	0.49	PL	0.13
14	C,D	%U	PL	0.43	PL	0.26
15	C,E	L/nL	PM	0.47	HP	0.33
16	C,F	%U	PL	0.58	PL	0.33
17	C,G	L/nL	PM	0.59	PL	0.30
18*	C,H	LL	HP	0.70	PL	0.26
19	D,E	LL	HP	0.47	PM	0.23

59

20	D,F	LL	HP	0.35	HP	0.31
21	D,G	%C	PL	0.26	HP	0.28
22	D,H	%U	PL	0.35	HP	0.22
23	A,B,C	LL	HP	0.47	PL	0.27
24	A,B,D	L/nL	HP	0.48	HP	0.15
25**	A,B,E	L/nL	HP	0.61	HP	0.26
26	A,B,F	L/nL	HP	0.41	PL	0.36
27	A,B,G	L/nL	PL	0.41	HP	0.34
28	A,B,H	%U	PL	0.55	HP	0.15
29	A,C,E	L/nL	HP	0.42	HP	0.24
30	A,C,F	LL	HP	0.41	HP	0.30
31	A,C,G	LL	HP	0.46	HP	0.28
32	A,C,H	LL	HP	0.64	PL	0.19
33	A,D,E	L/nL	HP	0.49	HP	0.18
34	A,D,F	L/nL	HP	0.29	PL	0.28
35	A,D,G	L/nL	PL	0.38	HP	0.26
36	A,D,H	%U	PL	0.46	HP	0.15
37	B,C,D	LL	PM	0.45	PL	0.25
38	B,C,E	L/nL	HP	0.39	HP	0.30
39	B,C,F	LL	PM	0.42	HP	0.29
40	B,C,G	%C	PM	0.43	HP	0.27
41	B,C,H	LL	HP	0.52	PL	0.25
42	B,D,E	L/nL	HP	0.46	HP	0.18
43	B,D,F	LL	PM	0.35	HP	0.28
44	B,D,G	LL	PM	0.30	HP	0.26
45	B,D,H	L/nL	HP	0.39	HP	0.15
46	C,D,E	LL	HP	0.31	PL	0.22
47	C,D,F	%U	PL	0.39	HP	0.22
48	C,D,G	%U	PL	0.39	HP	0.20
49	C,D,H	LL	HP	0.47	PL	0.17
50	A,B,C,D	L/nL	HP	0.36	PL	0.21
51	A,B,C,E	L/nL	HP	0.46	PL	0.24
52	A,B,C,F	LL	HP	0.35	HP	0.28
53	A,B,C,G	LL	HP	0.39	HP	0.26
54	A,B,C,H	LL	HP	0.52	PL	0.21
55	B,C,D,E	L/nL	HP	0.35	PL	0.23
56	B,C,D,F	LL	PM	0.39	HP	0.22
57	B,C,D,G	LL	PM	0.35	HP	0.20
58	B,C,D,H	LL	HP	0.39	PL	0.19
59	A,B,C,D,E	L/nL	HP	0.41	PL	0.19

60	A,B,C,D,F	LL	PM	0.31	HP	0.22
61	A,B,C,D,G	L/nL	PL	0.33	HP	0.21
62	A,B,C,D,H	LL	HP	0.42	PL	0.16

Supplemental Methods

Furfural concentration measurements

Furfural concentration was estimated according to the previously reported spectrophotometric method (Martinez et al., 2000).

Ethanol quantification by GC-FID

One milliliter of fermentation broth was centrifuged 3 min at 15 000g. The supernatant was collected and filtered with a syringe filter (0.45µm). Filtered volume was run through an Agilent CP8553 column (15 m, 320 µm, 0.5 µm) with a flow rate of 5 mL/min, initial temperature of 35C, temperature range of 265 °C, and pressure of 10.747 psi. Ethanol retention time (5.40 min) was determined with external standards which were run in the same batch as the samples and utilized to quantify ethanol for all analyzed samples.

Membrane lipid composition

Cultures growing at mid-log phase were centrifuged for 10 min at 4000 rpm (TX-1000 swinging bucket rotor) and 4 °C. Cell pellets were washed twice with 20 ml ice-cold sterile nanopure water, 6 ml of methanol were added to each washed pellet, the solution was gently mixed using a micropipette, and 1.4 ml of homogenized cells in methanol was transferred to a glass tube for each technical replicate of the lipid extraction method. Cells were lysed by sonication three times utilizing an FS110H sonicator (Thermo Fisher, Rockford IL). Each sonication consisted of a 20 s period of burst and a 20 s period of cooling on ice. Twenty microliters of a previously prepared mixture of C11/C15 fatty acids at a concentration of 1µg/µl each dissolved in methanol were added to each glass tube and utilized as the internal standard. Lysed cells were incubated at 70 °C for 15 min and centrifuged at 4000 rpm (TX-1000 swinging bucket rotor) for 5 min. For each tube, the supernatant was transferred to a new glass tube containing 1.4 ml of nanopure water. Likewise, the cell pellet was dissolved in 750 µl chloroform and incubated at 37 °C for 5 min. Later, the supernatant with water solution was added back into the cell pellet solution with chloroform. The resultant solution was vigorously

mixed, utilizing a Multi-Tube vortex (Thermo Scientific, Waltham MA) set at 2500 rpm for 2 min. The fatty acids interacted with aqueous and organic phases and migrated to the chloroform phase after homogenization and centrifugation at 3000 rpm (TX-1000 swinging bucket rotor) for 5 min.

Next, the extracted membrane fatty acids were derivatized into fatty acid methyl esters. For each tube, two milliliters of 1 N HCl in methanol were added to the extracted membrane fatty acids and incubated at 80 °C for 30 min. Two additional milliliters of 0.9% w/v NaCl, and 1 ml hexane were added and vigorously mixed. The solution was centrifuged at 2000g for 2 min, and the upper hexane phase was subjected to GC-MS analyses in the ISU Keck Laboratory facility. GC-MS was performed with an HP5 MSI (30 m, 0.250 mm, 0.25 µm) column, on a 780A gas chromatograph with a 5975C Agilent Mass Spectrophotometric Detector. Methanol and hexane were used as solvent washes solutions for the column at a flow rate of 300 µl/min. The oven of had an initial temperature of 50 °C with a rate of change of 25 °C/min. The equilibration time was 0.25 min, and the maximum temperature was 325 °C.

The total ion chromatogram peak areas were used to determine the abundance for each type of derivatized membrane fatty acid relative to the known moles of exogenously added internal standard C11/C15. The molar distribution for each type of fatty acid was converted to mass distribution and this is the percentage of the membrane lipid composition reported in this study. GC/MSD ChemStation software was utilized to analyze chromatograms, and the NIST MS Search 2.0 library was employed to identify the fragmentation patterns for each molecule. Determination of the different fatty acids, including positional isomers, was assessed by comparing their retention times and mass spectra.

Membrane fluidity

Cell densities of mid-log phase cultures were adjusted to achieve $OD_{550} = 1$ in 1 ml. Specifically, cells were centrifuged in 1.5 ml Eppendorf microcentrifuge tubes at 3800 g for 6 min. The cell pellet was washed twice with phosphate buffered saline (PBS) at pH 7.00 and resuspended in PBS to reach $OD_{550} \sim 0.1$. Each of the three biological replicates was divided into two technical replicates.

The probe 1,6- diphenyl-1,3,5-hexatriene (DPH) dissolved in dimethylformamide (DMF) (Sigma, St. Louis) was added to a final concentration of 0.4 µM to one of each of the two

technical replicates. Samples with and without DPH were incubated at 37 °C for 30 min and 200 rpm. The temperature of incubation was set to 42 °C instead to 37 °C when testing membrane fluidity of cultures grown at the higher temperature. After incubation, all samples were centrifuged at 3800 g for 6 min and resuspended in 500 µl of fresh PBS. One hundred microliters of cells were then placed into a dark-bottom flat 96-well plate with three technical replicates for each sample. We utilized the ISU Keck Laboratory facility for assessing membrane polarization utilizing a Synergy 2 multi-Mode microplate reader from BioTeK. The utilized filters were 360/40 nm and 460/40 nm for excitation and emission wavelengths, respectively. The excitation polarized filter was set in a vertical position while the emission polarized filter was set either in the vertical (I_{VV}) or horizontal (I_{VH}) position. These two values for I_{VV} and I_{VH} were calculated after the subtraction of the fluorescence values of the samples without DPH from the measured fluorescence values in samples with DPH. Thus, the fluorescence values as a consequence of only the DPH anisotropic probe were utilized for calculating the polarization ratio also known as the degree of fluorescence polarization.

$$P = \frac{I_{VV} - I_{VH}G}{I_{VV} + I_{VH}G}$$

Grating factor (G) was calculated as specified by BioTeK and was equal to $G = 1.1 \pm 0.1$. degree of fluorescence polarization in the intact cell membrane samples is inversely proportional to the cell membrane fluidity.

Membrane integrity

Seed cultures in MOPS 2% w/v dextrose were prepared as described for tolerance experiments. One hundred microliters of seed culture were centrifuged at 3800 g for 6 min, and cell pellets were washed once with 1 ml PBS. Cell suspensions were similarly centrifuged to form washed pellets. One milliliter of culture media with inhibitor was added to each washed pellet and gently mixed utilizing vortex. The volume from one tube was equally split into two tubes. One tube from each pair of replicates was treated with SYTOX Green to a final concentration of 5 µM, and the chemical was gently mixed utilizing vortex. Two hundred microliters of cells with SYTOX Green were placed in a well of a dark-bottom flat 96-well plate. The plate was incubated inside a SynergyHT BioTek microplate reader for 15 h at 37 ℃ and 307 cpm. Bulk fluorescence measurements were recorded every 20 min utilizing a filter of 485/20 nm and 516/20 nm for excitation and emission wavelengths, respectively. Fluorescence values

were obtained utilizing a gain value equal to 35 and the read height was 4.5 mm according to settings of SynergyHT BioTek microplate reader. Similarly, from the second tube of each replicate that does not contain SYTOX Green, two hundred microliters were placed in a well from a transparent bottom 96-well plate for measuring cell density (550 nm) every 20 min, for 15 h at 37 ºC and 307 cpm in an Eon Biotek microplate reader. Normalized fluorescence values were calculated at the same time (6 h) for all cultures. At this time, all cultures had their maximum OD_{550} while being still at exponential phase. These criteria were also considered for the other membrane characterization techniques. Membrane leakage values did not significantly change later in the culture for all conditions.

Membrane hydrophobicity

Twenty-five milliliters of mid-log phase culture were harvested by centrifugation at 4000 rpm (TX-1000 swinging bucket rotor) for 10 min in 50-ml centrifuge tubes. The cell pellets were washed twice with ice-cold PBS, and cell density (OD_{550}) was measured. The OD_{550} was adjusted to 0.6, and 2 ml of culture suspension was transferred to a glass tube containing 0.5 ml dodecane. Three experimental replicates were included for each biological sample. The cell suspensions with dodecane were vigorously mixed, utilizing a Multi-Tube vortex (Thermo Scientific, Waltham MA) at 2500 rpm for 10 min. After this homogenization step, samples were held at room temperature for 15 minutes to allow organic phase separation from the aqueous phase. Cell density OD_{550} was measured in the resulting aqueous phase containing the cells that did not migrate to the organic phase. The percentage of partition in the organic phase was calculated utilizing two OD_{550} values, before and after the homogenization step. This partitioning into the organic phase is the percentage of microbial adhesion to hydrocarbons (MATH). This value reports the percentage of cells from a sample that partitioned into the organic phase and it was used in this study as a metric of membrane hydrophobicity.

Supplementary references

Martinez, A., Rodriguez, M.E., York, S.W., Preston, J.F., Ingram, L.O., 2000. Use of UV absorbance to monitor furans in dilute acid hydrolysates of biomass. Biotechnol. Prog. 16, 637-641.